

# Semiparametric Functional Factor Models with Bayesian Rank Selection

Daniel R. Kowal\* and Antonio Canale†

## Abstract

Functional data are frequently accompanied by parametric templates that describe the typical shapes of the functions. Although the templates incorporate critical domain knowledge, parametric functional data models can incur significant bias, which undermines the usefulness and interpretability of these models. To correct for model misspecification, we augment the parametric templates with an infinite-dimensional nonparametric functional basis. Crucially, the nonparametric factors are regularized with an ordered spike-and-slab prior that provides consistent rank selection and satisfies several appealing theoretical properties. This prior is accompanied by a parameter expansion scheme customized to boost MCMC efficiency, and is broadly applicable for Bayesian factor models. The nonparametric basis functions are learned from the data, yet constrained to be orthogonal to the parametric template in order to preserve distinctness between the parametric and nonparametric terms. The versatility of the proposed approach is illustrated through applications to synthetic data, human motor control data, and dynamic yield curve data. Relative to parametric alternatives, the proposed semiparametric functional factor model eliminates bias, reduces excessive posterior and predictive uncertainty, and provides reliable inference on the effective number of nonparametric terms—all with minimal additional computational costs.

**KEYWORDS:** factor analysis; nonparametric regression; shrinkage prior; spike-and-slab prior; yield curve

---

\*Dobelman Family Assistant Professor, Department of Statistics, Rice University (daniel.kowal@rice.edu).

†Associate Professor, Department of Statistics, University of Padova (antonio.canale@unipd.it).

# 1 Introduction

## 1.1 Setting and goals

As high-resolution monitoring and measurement systems generate vast quantities of complex and highly correlated data, *functional data analysis* has become increasingly vital for many scientific, medical, business, and industrial applications. Functional data are (noisy) realizations of random functions  $\{Y_i\}_{i=1}^n$  observed over a continuous domain, such as time, space, or wavelength, and exhibit a broad variety of shapes. The concurrence of *complex* and *voluminous* data prompts the common use of nonparametric models for functional data. Yet in many cases, there is valuable information regarding the functional form of  $Y_i$ . Template curves that describe the shape of  $Y_i$  are derived from fundamental scientific laws or motivated by extensive empirical studies, and often are the focal point of the analysis. Prominent examples include human motor control (Ramsay, 2000; Ramsay et al., 1995; Goldsmith and Kitago, 2016), yield curves and interest rates (Nelson and Siegel, 1987; Diebold and Li, 2006), and basal body temperature (Scarpa and Dunson, 2009, 2014; Canale et al., 2017).

Our goal is to construct a functional data modeling framework that simultaneously (i) incorporates parametric templates in a coherent and interpretable manner, (ii) maintains the modeling flexibility of nonparametric methods, and (iii) provides computationally scalable inference with reliable uncertainty quantification. The approach is fully Bayesian, accompanied by an efficient MCMC algorithm for posterior and predictive inference, and equally applicable to both densely-observed and sparsely- or irregularly-sampled functional data.

The parametric templates are represented as a spanning set  $\mathcal{H}_0 = \text{span}\{g_1(\cdot; \gamma), \dots, g_L(\cdot; \gamma)\}$  of functions  $\{g_\ell(\cdot, \gamma)\}_{\ell=1}^L$  known up to  $\gamma$ . Any function belonging to  $\mathcal{H}_0$  is a linear combination of  $\{g_\ell\}$ ; the corresponding coefficients and the parameters  $\gamma$  must be learned. Important examples are presented in Table 1. The linear basis is routinely used for longitudinal data analysis and here is equivalent to a random slope model (Molenberghs and Verbeke, 2000).

A change in slope,  $(\tau - \gamma)_+$  with  $(x)_+ = \max\{0, x\}$ , is useful for modeling structural changes, such as a change in disease transmissions due to policy interventions (Wagner et al., 2020). Cosinor functions model circadian rhythms (Mikulich et al., 2003) and other periodic behaviors (Welham et al., 2006). Biphasic curves offer utility in modeling basal body temperature of women during the menstrual cycle (Scarpa and Dunson, 2009, 2014; Canale et al., 2017). In general, interest centers on learning the linear coefficients associated with each  $g_\ell$ , the nonlinear parameters  $\gamma$ , and an adequate yet interpretable model for the functions  $Y_i$ .

Linear	Linear change	Cosinor	Biphasic
$\{1, \tau\}$	$\{1, \tau, (\tau - \gamma)_+\}$	$\{1, \sin(2\pi\tau/\gamma), \cos(2\pi\tau/\gamma)\}$	$\{1, \exp(\gamma\tau)/\{1 + \exp(\gamma\tau)\}\}$

Table 1: Examples of parametric templates, or spanning sets, for  $\mathcal{H}_0$ .

The advantages of the parametric templates are clear: they incorporate domain knowledge, lend interpretability to the model, and often produce low-variance estimators relative to nonparametric alternatives. These templates are restrictive by design, and therefore can incur significant bias and other model misspecifications. Such effects erode model interpretability and can induce variance inflation. For illustration, we present model fits for two datasets in Figure 1 using a parametric model and our proposed semiparametric alternative; details and analyses of these data are in Section 6. In both instances, the templates capture the general shape of the data. However, regions of substantial bias are present, which produce uniformly inflated prediction bands over the domain. By comparison, the proposed approach preserves the essential shape of the curves, yet corrects the bias and shrinks the prediction bands appropriately—and crucially does so without overfitting.

## 1.2 Overview of the proposed approach

The *semiparametric functional factor model* (SFFM) bridges the gap between parametric and nonparametric functional data models. The SFFM augments a parametric template  $\mathcal{H}_0$

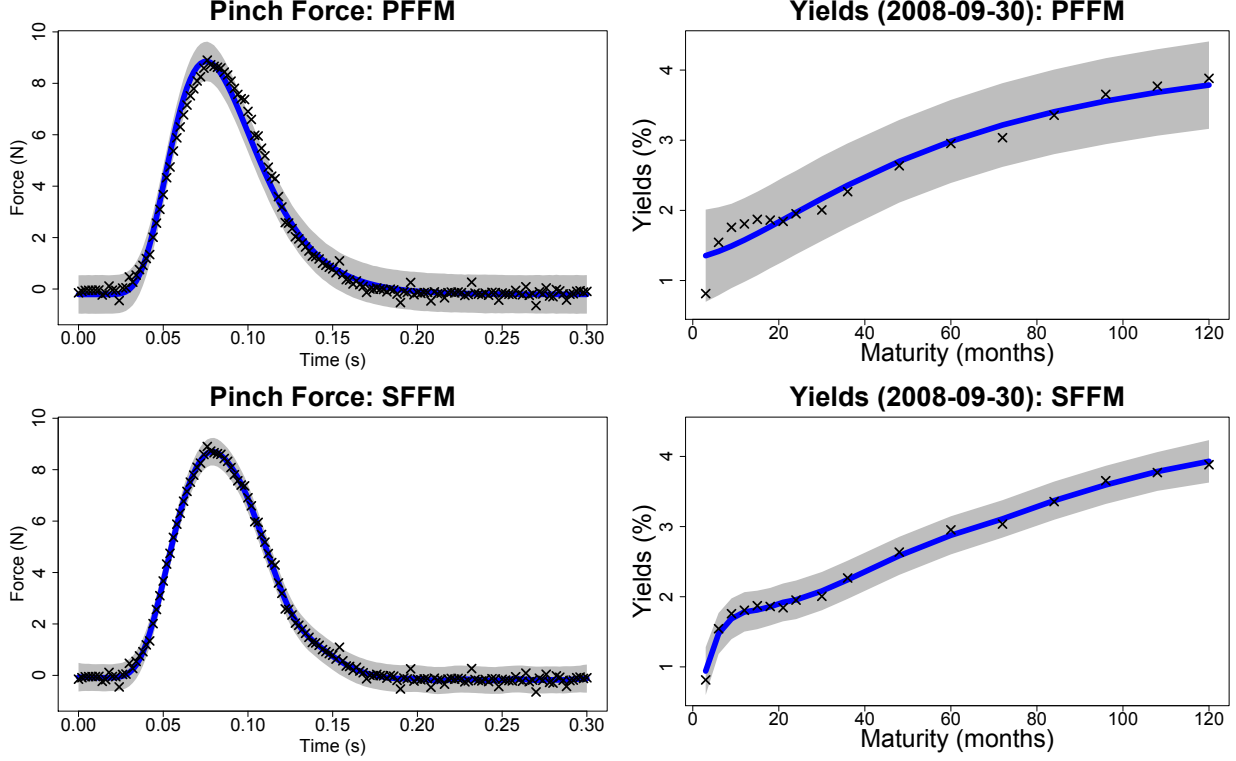


Figure 1: Posterior expectations and 95% simultaneous prediction bands for the parametric (PFFM, top) and semiparametric functional factor model (SFFM, bottom) for one replicate of the pinch force data (left; see Section 6.1) and one yield curve (right; see Section 6.2). The proposed SFFM corrects the bias of the PFFM and offers narrower prediction bands.

with a nonparametric and infinite-dimensional basis expansion for the functions  $Y_i \in L^2(\mathcal{T})$ :

$$Y_i(\tau) = \sum_{\ell=1}^L \alpha_{\ell,i} g_{\ell}(\tau; \gamma) + \sum_{k=1}^{\infty} \beta_{k,i} f_k(\tau), \quad \tau \in \mathcal{T}, \quad (1)$$

where  $\{f_k\}$  are unknown nonparametric functions,  $\{\alpha_{\ell,i}\}$  and  $\{\beta_{k,i}\}$  are unknown factors for the parametric and nonparametric components, respectively, and  $\mathcal{T} \subset \mathbb{R}^d$  is the domain, usually with  $d = 1$  for curves or  $d = 2$  for images. Without the nonparametric terms, (1) is a *parametric functional factor model* (PFFM), which serves as our parametric baseline.

Our implementation of (1) is fully Bayesian with three unique and essential features.

First, the nonparametric basis  $\{f_k\}$  is treated as unknown. The SFFM pools information

across all functions  $\{Y_i\}$  to learn the key functional features in the data—in particular, the systemic biases unresolved by  $\mathcal{H}_0$ . The functions  $\{f_k\}$  are learned jointly with the parametric terms  $\gamma$  and  $\{\alpha_{\ell,i}\}$  and the nonparametric factors  $\{\beta_{k,i}\}$ . A variety of models for each  $f_k$  are compatible within this framework, such as splines, wavelets, or Gaussian processes, while uncertainty about  $\{f_k\}$  is automatically absorbed into the joint posterior distribution.

Second, the nonparametric factors  $\{\beta_{k,i}\}$  are endowed with an ordered spike-and-slab prior distribution. The proposed prior is critical for coherence of the infinite-dimensional basis expansion in (1): it provides much-needed regularization, encourages selection of a finite number of factors, and provides posterior inference for the effective number of nonparametric terms—including an assessment of whether any nonparametric component is needed at all. The prior admits a parameter expansion that offers substantial improvements in MCMC efficiency and satisfies several key properties that broaden applicability beyond the SFFM.

Third, the nonparametric basis  $\{f_k\}$  is constrained to be orthogonal to the templates  $\{g_\ell\}$ . This important constraint enforces distinctness between the parametric and nonparametric components of the SFFM, which preserves the interpretability of the parametric model. The nonredundancy of  $\{f_k\}$  is also essential for valid inference on the effective number of nonparametric terms. As an added benefit, the orthogonality constraint produces computational simplifications that improve both the algorithmic efficiency and the ease of implementation of the MCMC algorithm.

The SFFM in (1) is accompanied by an observation error equation to accommodate noisy and sparsely- or irregularly-sampled functional data. The observed data  $\mathbf{y}_i = (y_{i,1}, \dots, y_{i,m_i})'$  are modeled as noisy realizations of  $Y_i$  on a discrete set of points  $\{\tau_{i,j}\}_{j=1}^{m_i} \subset \mathcal{T}$  for  $i = 1, \dots, n$ :

$$y_{i,j} = Y_i(\tau_{i,j}) + \epsilon_{i,j}, \quad \epsilon_{i,j} \overset{\text{indep}}{\sim} N(0, \sigma_\epsilon^2), \quad (2)$$

although non-Gaussian versions are available. We proceed using common observation points

$\tau_{i,j} = \tau_j$  and  $m_i = m$  for notational simplicity, but this restriction may be relaxed.

Although we focus on the parametric and semiparametric versions of (1), the proposed modeling framework remains useful without any parametric template ( $L = 0$ ). In this case, (1) resembles a Karhunen-Loève decomposition, and  $\{f_k\}$  correspond to the eigenfunctions of the covariance function of  $\{Y_i\}$  (assuming the functions  $Y_i$  have been centered). The Karhunen-Loève decomposition provides the theoretical foundation for functional principal components analysis (FPCA), which is widely used in functional data analysis. As such, model (1)—together with the model for  $\{f_k\}$  and the ordered spike-and-slab prior for  $\{\beta_{k,i}\}$ —constitutes a new approach for Bayesian FPCA or functional factor modeling.

### 1.3 Review of related approaches

Semiparametric models for functional data have appeared primarily in the frequentist literature. For modeling a single function, L-splines incorporate a favored space of parametric functions  $\mathcal{H}_0$  by combining a goodness-of-fit criterion with a penalty on deviations from  $\mathcal{H}_0$  (Ramsay and Dalzell, 1991; Heckman and Ramsay, 2000). The elegance of L-splines emanates from reproducing kernel Hilbert space (RKHS) theory: by specifying a RKHS and a penalty operator with null space  $\mathcal{H}_0$ , the Riesz representation theorem induces an expansion of the form (1), where only  $m$  basis functions  $\{f_k\}_{k=1}^m$  are needed and can be derived analytically (Wang, 2011). However, these derivations are highly challenging for all but the simplest choices of  $\mathcal{H}_0$ , which inhibits widespread practical use. In addition, L-splines offer limited direct inference on the adequacy of the parametric templates  $\mathcal{H}_0$ , and typically require hypothesis tests with asymptotic validity. By comparison, the proposed SFFM learns  $\{f_k\}_{k=1}^\infty$  directly from the data—which sidesteps the challenging derivations—and provides direct posterior inference on the effective number of nonparametric terms.

Other non-Bayesian approaches for semiparametric functional data analysis seek to replace nonparametric functions with parametric alternatives. Sang et al. (2017) attempt to

simplify FPCA by using polynomials for each FPC instead of splines or Fourier functions. In functional regression analysis, Chen et al. (2019) develop hypothesis tests to determine whether an unknown regression function deviates from a parametric template.

Bayesian semiparametric functional data models are less common. The “semiparametric” model of Lee et al. (2018) refers to additive rather than linear effects, but does not include a parametric template like  $\mathcal{H}_0$ . Scarpa and Dunson (2009) construct a Dirichlet process mixture of a parametric function and a Gaussian process contamination, which is generalized by Scarpa and Dunson (2014) to include prior information on the frequencies of certain functional features. These methods are designed primarily for clustering: they identify individual curves  $Y_i$  that deviate substantially from the parametric model, while the remaining curves are presumably well modeled parametrically. The SFFM is capable of modeling total deviations from  $\mathcal{H}_0$  for a particular  $Y_i$ , but also captures—and corrects—partial deviations from  $\mathcal{H}_0$  that persist for some or many  $Y_i$ . Unlike the mixture models, the SFFM is well suited for including additional layers of dependence, such as hierarchical (Section 6.1) or dynamic (Section 6.2) models, while maintaining efficient posterior computing.

Functional factor models such as (1) require rank selection. In FPCA, the rank is usually selected to explain a pre-specified proportion of variability in the data. This approach is not compatible with fully Bayesian inference and is complicated by the presence of the parametric templates in (1), which include unknown parameters. Information criteria offer metrics for model comparisons, but require separate model fits for each rank. Multiplicative gamma process priors (Bhattacharya and Dunson, 2011) can reduce sensitivity to the choice of the rank but can induce undesirable overshrinkage (Durante, 2017). The proposed ordered spike-and-slab prior resolves these issues and provides computationally efficient, interpretable, and consistent posterior inference on the rank of the nonparametric term.

Indian buffet processes (IBPs; Griffiths and Ghahramani, 2011) provide an alternative strategy for factor models that encourages both sparsity and rank selection. IBPs have been

applied successfully to (non-functional) Bayesian factor models, including regression (Rai and Daumé III, 2009), sparse point estimation (Ročková and George, 2016), and fully Bayesian inference with rank selection (Ohn and Kim, 2021). In the context of (1), IBPs are most commonly applied to the  $m \times \infty$  matrix  $\mathbf{F} = (\mathbf{f}_1, \mathbf{f}_2, \dots)$  where  $\mathbf{f}_k = (f_k(\tau_1), \dots, f_k(\tau_m))'$ . However, the IBP elementwise sparsity of  $\mathbf{F}$  is more appropriate for matrix factor models than functional factor models: setting  $f_k(\tau_j) = 0$  is usually less desirable than encouraging smoothness for  $f_k$ . Nonetheless, IBPs are intrinsically linked to the proposed ordered spike-and-slab prior, which we detail in Section 2.2.

The remainder of the paper is organized as follows. We introduce the ordered spike-and-slab prior in Section 2. The model for the parametric and nonparametric functions, including the constraints, is in Section 3. The MCMC algorithm is discussed in Section 4. A simulation study is in Section 5. The model is applied to real datasets in Section 6. We conclude in Section 7. Online supplementary material includes proofs of all theoretical results, the full MCMC algorithm, additional simulations, and R code for reproducibility.

## 2 Ordered spike-and-slab priors

The SFFM (1) augments the parametric template  $\mathcal{H}_0$  with a nonparametric component to reduce bias and model misspecification. These additional terms increase model complexity and should be removed whenever the added complexity is not supported by the data. This effort is related to rank selection, which seeks to identify a small number of necessary factors, yet is complicated by the presence of the parametric template with unknown  $\{\alpha_{\ell,i}\}$  and  $\gamma$ .

Leveraging the Bayesian framework, we design an ordered spike-and-slab prior for the nonparametric factors  $\{\beta_{k,i}\}$ . The spike-and-slab formulation provides joint shrinkage and selection for each  $\boldsymbol{\beta}_k = (\beta_{k,1}, \dots, \beta_{k,n})'$  and therefore removes unnecessary nonparametric factors from the model. We build upon the spike-and-slab prior of Ishwaran and Rao (2005)



for linear regression and extend this approach to the functional data setting. Compared to linear regression, model (1) is complicated significantly by the infinite-dimensional basis expansion. Our solution is to impose ordering in the spike-and-slab prior. Since additional factors are increasingly pulled toward the spike (inactive) component *a priori*, the posterior distribution is encouraged to concentrate on finite truncations of (1).

## 2.1 Cumulative shrinkage processes for ordered selection

To incorporate ordered shrinkage and selection into model (1), we build upon the *cumulative shrinkage process* (CUSP) proposed by Legramanti et al. (2020). CUSPs are sparsity-inducing priors for infinite sequences of parameters with a defined ordering. Suppose that the inclusion of the  $k$ th factor  $\beta_k$  is determined by a parameter  $\theta_k$ ; we provide additional details on our specification of  $\theta_k$  below. In the general case, CUSPs define a spike-and-slab prior for parameters  $\{\theta_k\}_{k=1}^\infty$  with a particular structure on the spike probabilities  $\{\pi_k\}_{k=1}^\infty$ :

$$[\theta_k | \pi_k] \sim P_k, \quad P_k = (1 - \pi_k)P_{slab} + \pi_k P_{spike} \quad (3)$$

$$\pi_k = \sum_{h=1}^k \omega_h, \quad \omega_h = \nu_h \prod_{\ell=1}^{h-1} (1 - \nu_\ell), \quad \nu_\ell \stackrel{iid}{\sim} \text{Beta}(\iota, \iota\kappa), \quad (4)$$

where  $P_{slab}$  is distribution of the slab (active) component and  $P_{spike}$  is the distribution of the spike (inactive) component. The hyperparameters of the CUSP are determined by the distributions  $P_{slab}$  and  $P_{spike}$  and the scalars  $\iota, \kappa > 0$ . Legramanti et al. (2020) restrict  $P_{spike} = \delta_{\theta_\infty}$  to be a point mass at some pre-specified value  $\theta_\infty$  and fix  $\iota = 1$  and  $\kappa = 5$ , where  $\kappa$  is the prior expected number of active components.

The ordering of the spike probabilities  $\{\pi_k\}_{k=1}^\infty$  in (4) implies a certain ordering for the prior distribution of the parameters  $\{\theta_k\}_{k=1}^\infty$  in (3), which we formalize in the following result:

**Proposition 1.** *For  $\varepsilon > 0$  and fixed  $\theta_0$ , let  $\mathbb{B}_\varepsilon(\theta_0) = \{\theta_k : |\theta_k - \theta_0| < \varepsilon\}$ . Prior (3)-(4)*

implies that  $\mathbb{P}(|\theta_k - \theta_0| \leq \varepsilon) < \mathbb{P}(|\theta_{k+1} - \theta_0| \leq \varepsilon)$  whenever  $P_{slab}\{\mathbb{B}_\varepsilon(\theta_0)\} < P_{spike}\{\mathbb{B}_\varepsilon(\theta_0)\}$ .

Intuitively, for any  $\theta_0$  that is favored under the spike distribution  $P_{spike}$  relative to the slab distribution  $P_{slab}$ , the CUSP prior (3)-(4) places greater mass around  $\theta_0$  as  $k$  increases. For spike-and-slab priors, we are most interested in  $\theta_0 = 0$ . The special case of Proposition 1 with  $P_{spike} = \delta_{\theta_\infty}$ ,  $\iota = 1$ , and  $\theta_0 = 0$  is proved by Legramanti et al. (2020).

For interpretability and efficient MCMC sampling, there is a convenient data augmentation of the CUSP prior (3). Let  $z_k \in \{1, \dots, \infty\}$  denote a categorical variable with  $\mathbb{P}(z_k = h | \omega_h) = \omega_h$ . The specification  $[\theta_k | z_k] \sim (1 - \mathbb{I}\{z_k \leq k\})P_{slab} + \mathbb{I}\{z_k \leq k\}P_{spike}$  induces (3) via marginalization over  $z_k$ . The number of active (slab) terms is therefore  $K^* = \sum_{k=1}^{\infty} \mathbb{I}\{z_k > k\}$ , with posterior inference available through the proposed MCMC sampling algorithm (see Algorithm 1). For model (1),  $K^*$  is the effective number of nonparametric terms, and therefore is an important inferential target to assess the adequacy of the parametric model.

The prior expected number of slab terms is  $\mathbb{E}(K^*) = \kappa$ , which appears in (4) and allows for the inclusion of prior information regarding the number of factors. The choice of  $\kappa$  can influence the posterior distribution for  $K^*$ , and thus subsequent inference on the number of nonparametric factors in (1). To mitigate this effect, we propose the hyperprior  $\kappa \sim \text{Gamma}(a_\kappa, b_\kappa)$  for  $a_\kappa, b_\kappa > 0$ , which is conditionally conjugate to (4). The hyperparameters may be selected to provide weak prior information regarding the number of factors: in practice, we set  $a_\kappa = 2$  and  $b_\kappa = 1$  so that  $\mathbb{E}(\kappa) = \text{Var}(\kappa) = 2$ . Similarly, we select the default value  $\iota = 1$  for simplicity.

To specify  $P_{slab}$  and  $P_{spike}$ , we apply a normal mixture of inverse-gamma (NMIG; Ishwaran and Rao, 2005) prior:

$$[\eta_k | \theta_k, \sigma_k^2] \stackrel{indep}{\sim} N(0, \theta_k \sigma_k^2), \quad [\theta_k | \pi_k] \sim (1 - \pi_k)\delta_1 + \pi_k\delta_{v_0}, \quad [\sigma_k^{-2}] \stackrel{iid}{\sim} \text{Gamma}(a_1, a_2) \quad (5)$$

where the scalars  $\{\eta_k\}$  are linked to the factors  $\{\beta_{k,i}\}$  in Section 2.4 and  $v_0$ ,  $a_1$  and  $a_2$  are hyperparameters. The NMIG prior incorporates variable selection by assigning the variance scale parameter  $\theta_k$  to the slab component,  $\theta_k = 1$ , or the spike component,  $\theta_k = v_0$ . By design, the NMIG prior produces a continuous distribution for the conditional variance of  $\eta_k$ , which is preferable for variable selection and risk properties (Ishwaran and Rao, 2005). Further, Ishwaran and Rao (2005) and Scheipl et al. (2012) note that the NMIG prior is less sensitive to hyperparameter choices compared to other spike-and-slab priors.

Consider the marginal prior for  $\eta_k$  in (5), conditional on  $\pi_k$ :

$$[\eta_k | \pi_k] \sim (1 - \pi_k)t_{2a_1}(0, \sqrt{a_2/a_1}) + \pi_k t_{2a_1}(0, \sqrt{v_0 a_2/a_1}) \quad (6)$$

where  $t_d(m, s)$  denotes a  $t$ -distribution with mean  $m$ , standard deviation  $s$ , and degrees of freedom  $d$ . By coupling (6) with the CUSP prior for  $\{\pi_k\}$  in (4), we obtain the following ordering result for the marginal prior on  $\{\eta_k\}_{k=1}^\infty$  (unconditional on  $\pi_k$ ):

**Corollary 1.** *For  $\varepsilon > 0$ ,  $\mathbb{P}(|\eta_k| \leq \varepsilon) < \mathbb{P}(|\eta_{k+1}| \leq \varepsilon)$  whenever  $v_0 < 1$ .*

Corollary 1 follows from Proposition 1 by observing that (6) is a special case of (3) and that the densities of the  $t$ -distributions in (3) place greater mass near zero when the scale parameter is smaller. The restriction  $v_0 < 1$  is self-evident, since it ensures that the spike distribution is indeed more concentrated around zero.

For practical implementation, it is advantageous to truncate the infinite summation in (1), which provides simpler and faster computations. The following result shows that finite approximations are accurate for sufficiently large truncation  $K$ :

**Proposition 2.** *Let  $\theta^{(K)} = \{\theta_k\}_{k=1}^K$  denote the sequence  $\{\theta_k\}_{k=1}^\infty$  truncated at  $K$ . For  $0 < v_0 < \varepsilon < 1$ , we have  $\mathbb{P}\{d_\infty(\theta, \theta^{(K)}) > \varepsilon\} \leq \kappa\{\kappa/(1 + \kappa)\}^K$ .*

The approximation error induced by truncating  $\{\theta_k\}_{k=1}^\infty$  to  $K$  terms decreases rapidly in  $K$ , which suggests that the proposed infinite-dimensional ordered spike-and-slab prior is

accurately approximated by a conservative truncation. Since we obtain inference for the effective number of active components,  $K^*$ , we can assess whether the posterior distribution of  $K^*$  places mass on values near  $K$ , which indicates that a larger value of  $K$  is necessary.

## 2.2 Connections to Indian Buffet Processes

The stick-breaking construction for  $\omega_h$  in (4) is most commonly used for Dirichlet processes (DPs; Ishwaran and James, 2001). A popular nonparametric Bayesian alternative is the Indian buffet process (IBP; Griffiths and Ghahramani, 2011), which defines a prior over binary matrices  $B = \{b_{j,k}\}$  with  $m$  rows and infinitely many columns. Specifically, the IBP is obtained by establishing the conditional distributions

$$[b_{j,k}|\mu_k] \stackrel{indep}{\sim} \text{Bernoulli}(\mu_k), \quad [\mu_k] \stackrel{iid}{\sim} \text{Beta}(\iota\kappa/K, \iota), \quad (7)$$

usually with  $\iota = 1$ , and then integrating over  $\{\mu_k\}$  with  $K \rightarrow \infty$  (the standard IBP notation has been adapted to match (4)).

The distinctions between DPs and IBPs are illuminated by the comparative stick-breaking representations. In contrast to the DP stick-breaking process for  $\{\omega_h\}$  in (4), the IBP stick-breaking process is defined by Teh et al. (2007) for the ordered (slab) probabilities  $\mu_{(1)} > \dots > \mu_{(K)}$ :

$$\mu_{(k)} = \prod_{\ell=1}^k \nu'_\ell, \quad \nu'_\ell \stackrel{iid}{\sim} \text{Beta}(\iota\kappa, \iota). \quad (8)$$

The DP stick lengths  $\{\omega_h\}$  sum to one but are not decreasing, while IBP stick lengths  $\{\mu_{(k)}\}$  do not necessarily sum to one but are decreasing.

By instead considering the *cumulative summation* in (4), we uncover a more direct connection with IBPs. Unlike the DP stick-breaking process, the cumulative summation for  $\pi_k$  ensures an increasing sequence of (spike) probabilities,  $\pi_k < \pi_{k+1}$ , that converges:

$\lim_{k \rightarrow \infty} \pi_k = 1$ . Most interesting, the CUSP probability sequence  $\{\pi_k\}_{k=1}^\infty$  has a simple mapping to the IBP stick-breaking construction:

**Proposition 3.** *The CUSP (4) satisfies  $(1 - \pi_k) = \mu_{(k)}$  where  $\mu_{(1)} > \dots > \mu_{(K)}$  are the ordered (slab) probabilities from the stick-breaking construction (8) of the IBP (7).*

Conventionally, IBPs apply the multiplicative beta process to the slab probability  $(1 - \pi_k)$ , which explains the complement in Proposition 3.

Despite these fundamental connections between  $\{\pi_k\}$  and  $\{\mu_{(k)}\}$ , CUSPs and IBPs remain distinct due to (3): CUSPs define a spike-and-slab prior for a sequence of parameters  $\{\theta_k\}_{k=1}^\infty$ , while IBPs define a prior over binary matrices  $B = \{b_{j,k}\}$ . In the context of (1), elementwise sparsity of  $\mathbf{F} = (\mathbf{f}_1, \mathbf{f}_2, \dots)$  for  $\mathbf{f}_k = (f_k(\tau_1), \dots, f_k(\tau_m))'$  is unwarranted: although we are interested in rank selection, we prefer priors that encourage smoothness rather than sparsity in  $f_k(\tau)$  over  $\tau \in \mathcal{T}$ .

## 2.3 Consistent rank selection for cumulative shrinkage processes

We investigate the asymptotic behavior of the posterior distribution for rank selection. Consider the modified setting with

$$y_i = \eta_{0i} + \epsilon_i, \quad \epsilon_i \stackrel{iid}{\sim} N(0, 1), \quad (9)$$

where  $\eta_{01}, \dots, \eta_{0n}$  are “true” mean parameters. This setting is related to the problem of estimating a high-dimensional mean vector from a single multivariate observation (Castillo and van der Vaart, 2012; Rockova, 2018), but we preserve the ordered sparsity:  $\eta_{0k} \neq 0$  for  $k \leq K_{0n}$  and  $\eta_{0k} = 0$  for  $k > K_{0n}$ . As such,  $K_{0n}$  is the true number of nonzero means and corresponds to the true rank in the SFFM model (1). Similarly, the dimension  $n$  can be considered equivalent to the upper truncation  $K$ . As customary in posterior asymptotics, we allow  $K_{0n}$  to grow with  $n$ .

We study the posterior of  $\eta_i$  under the NMIG prior in (5) and the CUSP in (3)-(4). A key term is the “remainder” for the CUSP,  $R_n = \sum_{k \geq K_{0n}} \omega_k$ , which represents an upper bound for the probability mass assigned to the slab for the parameters that are null. Under the CUSP, we show that  $R_n$  is far from zero with vanishing probability *a priori*:

**Lemma 1.** *Let  $\ell_n < \varepsilon_n < 1$  with  $\ell_n = (\kappa/(\kappa + 1))^{K_{0n}}$ . For the CUSP prior (3)-(4) and a positive constant  $C > 1$ , the remainder term  $R_n = \sum_{k \geq K_{0n}} \omega_k$  satisfies*

$$\mathbb{P}(R_n > \varepsilon_n) \leq \exp\{-CK_{0n}\}. \quad (10)$$

According to Lemma 3, the prior probability that  $R_n$  exceeds a small threshold is exponentially small. Such exponential decay in the prior is essential to obtain optimal posterior behavior in sparse settings (Castillo and van der Vaart, 2012). Note that this result does not require the NMIG prior.

To connect the prior behavior in Lemma 3 to the posterior, first consider the following mild conditions on the prior parameters: (C1)  $\sqrt{a_1/(a_2 v_0)} > K_{0n}/n$ ; (C2)  $AK_{0n}/n < 1/2$  with  $A > 1/2$ ; (C3)  $a_1 > 1/2$ , and  $a_1 \leq a_2$ . Condition (C1) implies that the squared proportion of nonzero parameters is smaller than the precision of the spike component; condition (C2) requires that  $K_{0n}$  is strictly less than the total number of elements (or the truncation limit); and condition (C3) implies that the values of the  $\sigma_k^2$  parameters in (5) are not too large. Now let  $\mathbb{P}_0$  and  $\mathbb{E}_0$  denote the probability and the expectation under the true distribution of the data (9), respectively. Under (C1)-(C3), the posterior probability that the remainder exceeds a shrinking  $\varepsilon_n$ , for  $n \rightarrow \infty$ , goes to zero in expectation  $\mathbb{E}_0$ :

**Theorem 1.** *Let  $\ell_n < \varepsilon_n < 1$  with  $\ell_n = (\kappa/(\kappa + 1))^{K_{0n}}$  and assume (C1)-(C3) and  $C > 2Ae$ . For the CUSP and NMIG priors, (3)-(4) and (5), respectively, the posterior satisfies  $\lim_{n \rightarrow \infty} \mathbb{E}_0 \{\mathbb{P}(R_n > \varepsilon_n \mid y_1, \dots, y_n)\} = 0$ .*

In the context of the SFFM, (9) can be obtained by treating the nonparametric basis  $\mathbf{F}$

as known and letting  $\beta_{k,i} = \eta_{k,i}$ . For simplicity, set the observation error variance in (1) to be  $\sigma_\epsilon^2 = n$ , which grows with the number of curves. The orthogonality of  $\mathbf{F}$  implies that the likelihood for  $\{\eta_k\}$  in (9) is equivalent to the likelihood implied by  $y_k = \bar{\eta}_k + \epsilon_k$  with  $\epsilon_k \stackrel{iid}{\sim} N(0, 1)$ , where  $y_k = n^{-1} \sum_{i=1}^n \mathbf{f}_k' \mathbf{y}_i$  is the projection of the functional data on the  $k$ th nonparametric basis function and averaged across the observed curves and  $\bar{\eta}_k = n^{-1} \sum_{i=1}^n \eta_{k,i}$ . The above results then apply assuming the NMIG prior for  $\{\bar{\eta}_k\}$  and by interchanging the notation  $k$  for  $n$ .

## 2.4 Parameter-expanded spike-and-slab models

The CUSP prior provides an appealing mechanism for introducing ordered shrinkage and selection into model (1). A subtle yet important feature of this framework is that spike-and-slab selection is applied jointly to the entire  $n$ -dimensional *vector*  $\boldsymbol{\beta}_k = (\beta_{k,1}, \dots, \beta_{k,n})'$ . However, parametrization of a vector  $\boldsymbol{\beta}_k$  in terms of a spike-and-slab prior on a scalar  $\eta_k$  is known to introduce significant challenges for MCMC sampling. Scheipl et al. (2012) show that as the dimension of the parameter vector increases, it becomes increasingly more difficult for the MCMC algorithm to switch between the slab and spike components. The consequences are nontrivial: without the ability to traverse between the slab and spike components, the uncertainty quantification for each factor's activeness is invalidated, and inference for the effective number of nonparametric factors  $K^*$  cannot proceed.

To illustrate, we compare the proposed approach to Legramanti et al. (2020), which uses CUSP priors but does not address this issue. We adopt the simulation design from Section 5 with  $K_{true} = 6$  nonparametric factors. The analogous prior in Legramanti et al. (2020) is  $[\beta_{k,i} | \theta_k] \stackrel{indep}{\sim} N(0, \theta_k)$  and a CUSP prior for  $\{\theta_k\}_{k=1}^\infty$  with  $P_{spike} = \delta_{\theta_\infty}$  and  $P_{slab} = \text{Inv-Gamma}(a_\theta, b_\theta)$ . We use the hyperparameters from Legramanti et al. (2020):  $\theta_\infty = 0.05$ ,  $a_\theta = b_\theta = 2$ , and  $\kappa = 5$ , but the subsequent results persist for other choices.

Figure 2 displays the MCMC samples of  $K^*$  across five different MCMC runs with random

initializations. The proposed approach produces draws that are centered at the true value with some variability:  $K^*$  changes values in 32% of the MCMC iterations. By comparison, the Legramanti et al. (2020) prior and sampler produces MCMC draws that are essentially stuck at a single value:  $K^*$  changes values in only 0.004% of the MCMC iterations. Clearly, the latter results cannot be used to provide reliable posterior uncertainty quantification for the effective number of nonparametric components  $K^*$ . Further, the proposed approach is more accurate: we estimate  $\mathbb{E}(K^*|\mathbf{y}) = 6.04$  for the proposed approach and  $\mathbb{E}(K^*|\mathbf{y}) = 4.84$  for the Legramanti et al. (2020) prior.

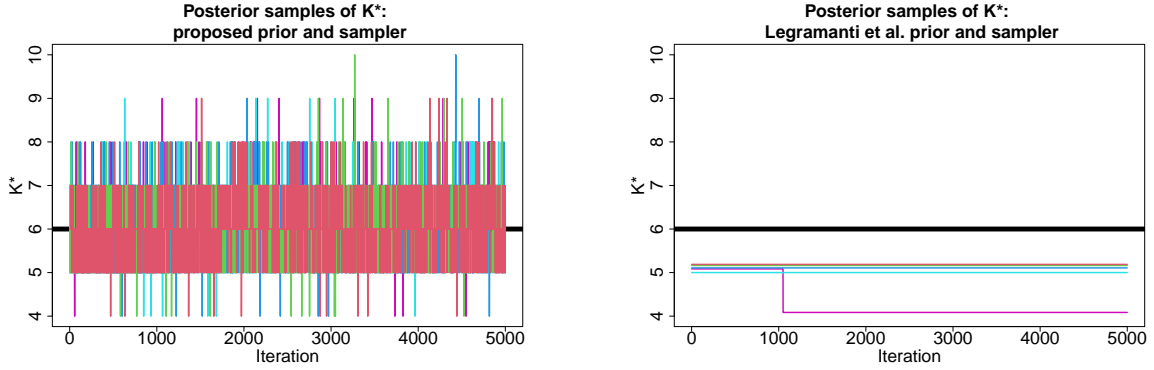


Figure 2: MCMC samples of  $K^*$  across 5 chains for the proposed prior and algorithm (left) compared to Legramanti et al. (2020) (right). The horizontal black line denotes the true value  $K_{true} = 6$ . The proposed approach provides substantial improvements in mixing and produces more accurate estimates.

Our solution is to introduce a redundant parameter expansion for the ordered spike-and-slab prior. We induce a prior on each factor  $\beta_{k,i}$  via the following parameter expansion:

$$\beta_{k,i} = \eta_k \xi_{k,i}, \quad [\xi_{k,i} | m_{\xi_{k,i}}] \stackrel{indep}{\sim} N(m_{\xi_{k,i}}, 1), \quad m_{\xi_{k,i}} \stackrel{indep}{\sim} \frac{1}{2}\delta_1 + \frac{1}{2}\delta_{-1} \quad (11)$$

where  $\eta_k$  applies the ordered spike-and-slab shrinkage for factor  $k$  via the NMIG prior (5) and  $\{\xi_{k,i}\}_{i=1}^n$  disperses this shrinkage throughout  $\{\beta_{k,i}\}_{i=1}^n$ . Here,  $\xi_{k,i}$  is nonidentifiable and exists primarily for the purpose of improving MCMC performance. The Gaussian parameter



expansion of  $\xi_{k,i}$  resembles Gelman (2006), yet is centered around 1 or  $-1$  with variance 1. As a result, the parameter  $\eta_k$  retains the interpretability as a selection parameter and assigns the magnitude to  $\beta_k$ .

The key distinction between the proposed prior and Scheipl et al. (2012) is the ordering implied by the prior for  $\{\pi_k\}_{k=1}^\infty$  given in (4). Direct application of Scheipl et al. (2012), in which the  $\pi_k$  probabilities in (5) are common for all  $k$  and assigned a Beta prior, is not appropriate for model (1): that approach does not provide ordered shrinkage or selection and is not designed to accommodate growing model dimension with an implicit ordering. Crucially, the parameter-expanded prior (11) maintains the required ordering on the factors:

**Proposition 4.** *For  $\varepsilon > 0$ ,  $\mathbb{P}(|\beta_{k,i}| \leq \varepsilon) < \mathbb{P}(|\beta_{k+1,i}| \leq \varepsilon)$  whenever  $v_0 < 1$ .*

Proposition 4 requires only that  $\{\xi_{k,i}\}$  are marginally independent and identically distributed. Therefore, other parameter expansion schemes may be substituted in (11) without disrupting the probabilistic ordering of  $|\beta_{k,i}|$ . By a similar argument, the ordering also is preserved across observations:  $\mathbb{P}(|\beta_{k,i}| \leq \varepsilon) < \mathbb{P}(|\beta_{k+1,i'}| \leq \varepsilon)$  for  $\varepsilon > 0$  and  $v_0 < 1$ .

## 3 Models and constraints for the basis functions

### 3.1 Model for the nonparametric functions

The error-free latent functions  $\{Y_i\}$  belong to the space spanned by the template parametric curves  $\{g_\ell\}$  and the nonparametric curves  $\{f_k\}$ . Any systemic bias resulting from the inadequacies of  $\{g_\ell\}$  must be corrected by  $\{f_k\}$ , which demands substantial flexibility of the nonparametric basis  $\{f_k\}$ . However, interpretability of the parametric terms  $\{g_\ell\}$  and  $\{\alpha_{\ell,i}\}$  requires a strict distinction between the parametric and nonparametric components.

To achieve both flexibility and distinctness, we model each  $f_k$  as a smooth unknown function such that each  $f_k$  is orthogonal to  $\{g_\ell\}$ . The model for  $f_k$  can be any Bayesian

curve-fitting model, such as splines, wavelets, or Gaussian processes, usually with a prior that encourages smoothness. The orthogonality constraints ensure nonredundancy of  $\{f_k\}$  and offer key computational simplifications that improve scalability and increase MCMC efficiency. These results maintain regardless of the specification of  $\{g_\ell\}$  or  $\{f_k\}$ .

Let  $f_k(\tau) = \mathbf{b}'(\tau)\boldsymbol{\psi}_k$  be a linear combination of known basis functions  $\mathbf{b}$  and unknown coefficients  $\boldsymbol{\psi}_k$ . We use low-rank thin plate splines for  $\mathbf{b}$ , which are flexible, computationally efficient, and well-defined on  $\mathcal{T} \subset \mathbb{R}^d$  for  $d \in \mathbb{Z}^+$ . The prior on each vector of basis coefficients  $\boldsymbol{\psi}_k$  is specified to encourage smoothness of  $f_k$ , akin to a classical spline roughness penalty:  $[\boldsymbol{\psi}_k | \lambda_{f_k}] \stackrel{\text{indep}}{\sim} N(\mathbf{0}, \lambda_{f_k}^{-1} \boldsymbol{\Omega}^-)$  where  $\lambda_{f_k}^{-1/2} \stackrel{\text{indep}}{\sim} \text{Uniform}(0, 10^4)$  is the prior precision and  $\boldsymbol{\Omega}$  is a known (roughness) penalty matrix. We select  $\boldsymbol{\Omega}$  to be the matrix of integrated squared second derivatives,  $[\boldsymbol{\Omega}]_{j,j'} = \int \ddot{b}_j(\tau) \ddot{b}_{j'}(\tau) d\tau$ , which implies that the prior distribution satisfies  $-2 \log p(\boldsymbol{\psi}_k | \lambda_{f_k}) \stackrel{c}{=} \lambda_{f_k} \boldsymbol{\psi}_k' \boldsymbol{\Omega} \boldsymbol{\psi}_k = \lambda_{f_k} \int \{\ddot{f}_k(\tau)\}^2 d\tau$  and  $\stackrel{c}{=}$  denotes equality up to a constant. The prior operates as a roughness penalty with an unknown smoothing parameter  $\lambda_{f_k}$  that is learned from the data. For more convenient and efficient computing, standard reparametrizations can diagonalize the penalty matrix  $\boldsymbol{\Omega}$  and orthogonalize the basis matrix  $\mathbf{B} = (\mathbf{b}'(\tau_1), \dots, \mathbf{b}'(\tau_m))'$  (Kowal, 2020). Details on low-rank thin plate splines and generalizations for  $d > 1$  are given in Wood (2006).

### 3.2 Orthogonality of the parametric and nonparametric functions

Orthogonality of the joint basis  $\{g_1, \dots, g_L, f_1, f_2, \dots\}$  is decomposed into three sets of constraints: orthogonality of the parametric basis  $\{g_\ell\}_{\ell=1}^L$ , orthogonality of the nonparametric basis  $\{f_k\}_{k=1}^\infty$ , and orthogonality between each parametric function  $g_\ell$  and nonparametric function  $f_k$ . Consider model (1)-(2) evaluated at the observation points  $\{\tau_j\}_{j=1}^m$ :

$$\mathbf{y}_i = \mathbf{G}_\gamma \boldsymbol{\alpha}_i + \mathbf{F} \boldsymbol{\beta}_i + \boldsymbol{\epsilon}_i, \quad \boldsymbol{\epsilon}_i \stackrel{\text{indep}}{\sim} N(\mathbf{0}, \sigma_\epsilon^2 \mathbf{I}_m), \quad i = 1, \dots, n \quad (12)$$

where  $\boldsymbol{\alpha}_i = (\alpha_{1,i}, \dots, \alpha_{L,i})'$ ,  $\mathbf{F} = (\mathbf{f}_1, \dots, \mathbf{f}_K)$  for  $\mathbf{f}_k = (f_k(\tau_1), \dots, f_k(\tau_m))' = \mathbf{B}\boldsymbol{\psi}_k$ , and  $\boldsymbol{\beta}_i = (\beta_{1,i}, \dots, \beta_{K,i})'$ . Here, we have truncated the CUSP prior at some conservative upper bound  $K$  as justified by Proposition 2.

The parametric matrix  $\mathbf{G}_\gamma$  is constructed and orthogonalized using a QR decomposition. For any value of  $\gamma$ , let  $\mathbf{G}_\gamma^0 = \mathbf{Q}_\gamma \mathbf{R}_\gamma$  be the QR decomposition of the initial basis matrix  $\mathbf{G}_\gamma^0 = (\mathbf{g}_{1;\gamma}, \dots, \mathbf{g}_{L;\gamma})$  with  $\mathbf{g}_{\ell;\gamma} = (g_\ell(\tau_1; \gamma), \dots, g_\ell(\tau_m; \gamma))'$ . By setting  $\mathbf{G}_\gamma = \mathbf{Q}_\gamma$ , we ensure that  $\mathbf{G}_\gamma' \mathbf{G}_\gamma = \mathbf{I}_L$  and the columns of  $\mathbf{G}_\gamma$  span the same space as the columns of  $\mathbf{G}_\gamma^0$ . When  $\gamma$  is unknown and endowed with a prior distribution, the QR decomposition is incorporated into the likelihood evaluations of (12) for posterior sampling of  $\gamma$ .

The nonparametric basis matrix  $\mathbf{F}$  is constrained such that  $\mathbf{F}' \mathbf{F} = \mathbf{I}_K$  and  $\mathbf{G}_\gamma' \mathbf{F} = \mathbf{0}_{L \times K}$ . The latter constraint is vital, and factors the likelihood (12) into parametric and nonparametric terms:

**Lemma 2.** *When  $\mathbf{G}_\gamma' \mathbf{F} = \mathbf{0}_{L \times K}$ , the likelihood (12) factorizes:  $p(\mathbf{y}|\gamma, \{\boldsymbol{\alpha}_i\}, \mathbf{F}, \{\boldsymbol{\beta}_i\}, \sigma_\epsilon^2) = p_0(\mathbf{y}|\gamma, \{\boldsymbol{\alpha}_i\}, \sigma_\epsilon^2) p_1(\mathbf{y}|\mathbf{F}, \{\boldsymbol{\beta}_i\}, \sigma_\epsilon^2)$ , where  $p_0$  depends on the parametric terms,  $\gamma$  and  $\{\boldsymbol{\alpha}_i\}$ , and the error variance  $\sigma_\epsilon^2$ , and  $p_1$  depends on the nonparametric terms,  $\mathbf{F}$  and  $\{\boldsymbol{\beta}_i\}$ , and  $\sigma_\epsilon^2$ .*

Within a Bayesian model, a reasonable notion of distinctness between parametric and nonparametric components is (conditional) independence in the posterior. By assuming independence in the prior, Lemma 2 ensures this result:

**Corollary 2.** *Suppose the parametric and nonparametric factors are a priori independent:  $p(\{\boldsymbol{\alpha}_i\}, \{\boldsymbol{\beta}_i\}) = p(\{\boldsymbol{\alpha}_i\})p(\{\boldsymbol{\beta}_i\})$ . Under model (12) and subject to  $\mathbf{G}_\gamma' \mathbf{F} = \mathbf{0}_{L \times K}$ , the parametric and nonparametric factors are a posteriori independent,  $p(\{\boldsymbol{\alpha}_i\}, \{\boldsymbol{\beta}_i\}|\mathbf{y}, \sigma_\epsilon^2, \mathbf{F}, \gamma) = p(\{\boldsymbol{\alpha}_i\}|\mathbf{y}, \sigma_\epsilon^2, \mathbf{F}, \gamma)p(\{\boldsymbol{\beta}_i\}|\mathbf{y}, \sigma_\epsilon^2, \mathbf{F}, \gamma)$ , conditional on  $\sigma_\epsilon^2, \mathbf{F}, \gamma$ .*

The consequences of Corollary 2 are important for posterior inference: by constraining the unknown nonparametric curves  $\mathbf{F}$  to be orthogonal to  $\mathbf{G}_\gamma$ , we ensure that the sampling steps for all parametric factors  $\{\boldsymbol{\alpha}_i\}$  do *not* depend on the nonparametric parameters in any

way. In particular, the sampling steps for  $\{\alpha_i\}$  are identical to the fully parametric case, while the sampling steps for  $\{\beta_i\}$  proceed exactly as in a fully nonparametric setting. This decoupling of parametric and nonparametric sampling steps is crucial for accommodating increases in model complexity.

### 3.3 Enforcing the orthogonality constraints

For each  $f_k$ , the orthogonality constraints are enforced in two stages: (i) the linear constraints  $\mathbf{G}'_\gamma \mathbf{f}_k = \mathbf{0}_L$  and  $\mathbf{f}'_{k'} \mathbf{f}_k = 0$  for  $k' \neq k$  are *conditioned upon* and (ii) the unit norm constraint  $\mathbf{f}'_k \mathbf{f}_k = 1$  is satisfied via normalization after sampling. The full conditional distribution for each  $\psi_k$  is  $N(\mathbf{Q}_{\psi_k}^{-1} \ell_{\psi_k}, \mathbf{Q}_{\psi_k}^{-1})$  for  $k = 1, \dots, K$ , where  $\mathbf{Q}_{\psi_k} = \sigma_\epsilon^{-2}(\mathbf{B}'\mathbf{B}) \sum_{i=1}^n \beta_{k,i}^2 + \lambda_{f_k} \mathbf{\Omega}$  and  $\ell_{\psi_k} = \sigma_\epsilon^{-2} \mathbf{B}' \sum_{i=1}^n \{\beta_{k,i}(\mathbf{y}_i - \mathbf{G}_\gamma \alpha_i - \sum_{\ell \neq k} \mathbf{f}_\ell \beta_{\ell,i})\}$ . The joint linear constraints are  $\mathbf{C}_k \psi_k = \mathbf{0}$  with  $\mathbf{C}_k = (\mathbf{G}_\gamma, \mathbf{f}_1, \dots, \mathbf{f}_{k-1}, \mathbf{f}_{k+1}, \dots, \mathbf{f}_K)' \mathbf{B}$ , which is linear in  $\psi_k$ ; conditioning on this constraint produces another Gaussian distribution. Samples from this distribution are easy to obtain: given a draw  $\psi_k^0 \sim N(\mathbf{Q}_{\psi_k}^{-1} \ell_{\psi_k}, \mathbf{Q}_{\psi_k}^{-1})$  from the unconstrained full conditional distribution, the vector  $\psi_k = \psi_k^0 - \mathbf{Q}_{\psi_k}^{-1} \mathbf{C}'_k (\mathbf{C}_k \mathbf{Q}_{\psi_k}^{-1} \mathbf{C}'_k)^{-1} \mathbf{C}_k \psi_k^0$  constitutes a draw from the full conditional distribution subject to the orthogonality constraints (Kowal, 2020). After drawing  $\psi_k$ , we rescale both  $\psi_k$  and  $\beta_{k,i}$  to enforce the unit-norm constraint while preserving the product  $\mathbf{f}_k \beta_{k,i}$  in the likelihood (12). This operation does not change the shape of the curve  $f_k$  nor the likelihood (12). Most important, the constraints  $\mathbf{G}'_\gamma \mathbf{F} = \mathbf{0}_{L \times K}$  and  $\mathbf{F}' \mathbf{F} = \mathbf{I}_K$  hold at every MCMC iteration.

## 4 MCMC for posterior inference

We design an efficient MCMC algorithm for posterior inference. The efficiency of the algorithm derives from two key features: the parameter-expanded sampler for the ordered spike-and-slab prior, which substantially improves MCMC mixing (see Figure 2), and the

orthogonality constraints on  $\{g_\ell\}$  and  $\{f_k\}$ , which produce important computational simplifications. The full MCMC algorithm is detailed in the supplementary material.

Algorithm 1 presents the sampling steps for the ordered spike-and-slab parameters. These steps consist of simple, fast, and closed form updates. The full conditionals depend on the data only through  $y_{k,i}^F = \mathbf{f}_k' \mathbf{y}_i$ , which offers an implicit dimension reduction from  $m$  to  $K$  and does not involve the parametric terms. These simplifications are a direct consequence of the orthogonality constraints. In addition, we retain posterior samples of  $K^* = \sum_{k=1}^K \mathbb{I}\{z_k > k\}$ , which is the effective number of nonparametric terms. Adaptations of this sampling algorithm for use of the ordered spike-and-slab prior with other models, such as (non-functional) factor models, are available by replacing  $y_{k,i}^F$  with the appropriate term.

---

**Algorithm 1:** MCMC sampling steps for the ordered spike-and-slab prior

---

Let  $y_{k,i}^F = \mathbf{f}_k' \mathbf{y}_i$  for  $i = 1, \dots, n$  and  $k = 1, \dots, K$ :

1. **Sample**  $[m_{\xi_{k,i}} | -]$  from  $\{-1, 1\}$  with  $\mathbb{P}(m_{\xi_{k,i}} = 1 | -) = 1 / \{1 + \exp(-2\xi_{h,i})\}$ ;
2. **Sample**  $[\xi_{k,i} | -] \sim N(Q_{\xi_{k,i}}^{-1} \ell_{\xi_{k,i}}, Q_{\xi_{k,i}}^{-1})$  where  $Q_{\xi_{k,i}} = \eta_k^2 / \sigma_\epsilon^2 + 1$  and  $\ell_{\xi_{k,i}} = \eta_k y_{k,i}^F / \sigma_\epsilon^2 + m_{\xi_{k,i}}$ ;
3. **Sample**  $[\eta_k | -] \sim N(Q_{\eta_k}^{-1} \ell_{\eta_k}, Q_{\eta_k}^{-1})$  where  $Q_{\eta_k} = \sum_{i=1}^n \xi_{k,i}^2 / \sigma_\epsilon^2 + (\theta_k \sigma_k^2)^{-1}$  and  $\ell_{\eta_k} = \sum_{i=1}^n \xi_{k,i} y_{k,i}^F / \sigma_\epsilon^2$ ;
4. **Rescale**  $\eta_k \rightarrow (\sum_{i=1}^n |\xi_{k,i}| / n) \eta_k$  and  $\boldsymbol{\xi}_k \rightarrow (n / \sum_{i=1}^n |\xi_{k,i}|) \boldsymbol{\xi}_k$  and **update**  $\beta_{k,i} = \xi_{k,i} \eta_k$ ;
5. **Sample**  $[\sigma_k^{-2} | -] \sim \text{Gamma}\{a_1 + 1/2, a_2 + \eta_k^2 / (2\theta_k)\}$ ;
6. **Sample**  $[\nu_k | -] \sim \text{Beta}(1 + \sum_{h=1}^K \mathbb{I}\{z_h = k\}, \kappa + \sum_{h=1}^K \mathbb{I}\{z_h > k\})$  for  $k = 1, \dots, K-1$  and **update**  $\pi_k$  and  $\omega_k$  from (4);
7. **Sample**  $[\kappa | -] \sim \text{Gamma}\{a_\kappa + K - 1, b_\kappa - \sum_{k=1}^{K-1} \log(1 - \nu_k)\}$ ;
8. **Sample**  $[z_k | -]$  from

$$\mathbb{P}(z_k = h | -) \propto \begin{cases} \omega_h t_{2a_1}(\eta_k; 0, \sqrt{v_0 a_2 / a_1}) & h \leq k \\ \omega_h t_{2a_1}(\eta_k; 0, \sqrt{a_2 / a_1}) & h > k \end{cases}$$

where  $t_d(x; m, s)$  is the density of the  $t$ -distribution evaluated at  $x$  with mean  $m$ , standard deviation  $s$ , and degrees of freedom  $d$ ;

9. **Update**  $\theta_k = 1$  if  $z_k > k$  and  $\theta_k = v_0$  if  $z_k \leq k$ .
-

The sampling steps for the nonparametric functions  $\{\mathbf{f}_k\}$  subject to orthogonality constraints are discussed in Section 3.3. Here, we note that these constraints pay dividends for efficient sampling of the parametric factors. Consider the prior  $\alpha_{\ell,i} \stackrel{indep}{\sim} N(0, \sigma_{\alpha_\ell}^2)$ ; alternative priors (see Section 6.2) benefit similarly. The full conditional distribution is simply  $[\boldsymbol{\alpha}_i | -] \stackrel{indep}{\sim} N(\mathbf{Q}_{\alpha_i}^{-1} \boldsymbol{\ell}_{\alpha_i}, \mathbf{Q}_{\alpha_i}^{-1})$  for  $i = 1, \dots, n$ , where  $\mathbf{Q}_{\alpha_i} = \sigma_\epsilon^{-2} \mathbf{I}_L + \text{diag}(\{\sigma_{\alpha_\ell}^{-2}\}_{\ell=1}^L)$  and  $\boldsymbol{\ell}_{\alpha_i} = \sigma_\epsilon^{-2} \mathbf{G}'_\gamma \mathbf{y}_i$ . The parametric factors are conditionally independent and do not involve any of the nonparametric terms, and therefore can be sampled jointly and efficiently.

## 5 Simulation study

We conduct a simulation study to assess model performance for (i) point and interval prediction of  $Y_i$  and  $\mathbf{y}_i$ , (ii) estimation and inference for the parametric coefficients  $\{\boldsymbol{\alpha}_i\}$ , and (iii) uncertainty quantification for the number of nonparametric terms. We focus on the linear template  $\mathcal{H}_0 = \text{span}\{1, \tau\}$  and present results for the Nelson-Siegel template with unknown  $\gamma$  in the supplementary material.

Synthetic functional data with  $n = 100$  curves and  $m = 25$  equally-spaced observation points in  $[0, 1]$  are generated as follows. The parametric and nonparametric factors are simulated as  $\alpha_{\ell,i}^* \stackrel{iid}{\sim} N(0, 1)$  and  $\beta_{k,i}^* \stackrel{indep}{\sim} N(0, 1/(k+1)^2)$ , respectively, for  $k = 1, \dots, K_{true}$  and  $K_{true} \in \{0, 1, 3, 8\}$ . By design, the variability in the parametric factors outweighs the variability in the nonparametric factors. The parametric basis matrix  $\mathbf{G}_\gamma^*$  is constructed by evaluating  $\{g_\ell\}$  at each observation point and QR-decomposing the resulting matrix as in Section 3.2. For the nonparametric functions  $f_k^*$ , we use orthogonal polynomials of degree  $k+1$ , which are orthogonal to the linear template; the Nelson-Siegel version requires an additional QR-based orthogonalization step. The error-free latent functions are  $\mathbf{Y}_i^* = \mathbf{G}_\gamma^* \boldsymbol{\alpha}_i^* + \mathbf{F}^* \boldsymbol{\beta}_i^*$  and the functional observations are generated as  $\mathbf{y}_i = \mathbf{Y}_i^* + \sigma^* \boldsymbol{\epsilon}_i^*$  where  $\sigma^* = \text{sd}(\mathbf{Y}_i^*)/\text{RSNR}$  for sample standard deviation  $\text{sd}(\cdot)$ , root signal-to-noise ratio  $\text{RSNR} = 3$ ,

and  $\epsilon_i^* \stackrel{iid}{\sim} N(\mathbf{0}, \mathbf{I}_m)$ . This process was repeated to create 100 synthetic datasets.

In addition to the PFFM and SFFM, we include a finite mixture model variant of the SFFM (SFFM-fmm) that instead assumes  $\omega_{1:K} \sim \text{Dirichlet}(\kappa/K, \dots, \kappa/K)$ . We use the same choice of  $K$  as in the SFFM (see below) and set the prior expected number of factors to be  $\kappa = 1$  to encourage fewer factors. As a secondary competitor, we include a Gaussian process modification (PFFM-gp) of (1):  $Y_i(\tau) = \sum_{\ell=1}^L \alpha_{\ell,i} g_\ell(\tau; \gamma) + X_i(\tau)$  with  $[X_i | \mathcal{K}_X] \stackrel{iid}{\sim} GP(0, \mathcal{K}_X)$ , which models each  $Y_i$  as a Gaussian process centered at the parametric template. For computational tractability, we use a standard functional data basis expansion  $X_i(\tau) = \mathbf{b}'(\tau) \chi_i$  where  $\mathbf{b}$  is a low-rank thin plate spline basis (see Section 3.1) and  $\chi_{i,r} \stackrel{iid}{\sim} N(0, \sigma_\chi^2)$  with  $\sigma_\chi \sim C^+(0, 1)$ . This representation induces a (conditional) Gaussian process for each  $X_i$ , but does not provide direct inference on  $K^*$  for rank selection.

For all models, we assume the conditionally Gaussian likelihood (12) with the hierarchical priors

$$[\alpha_{\ell,i} | \sigma_{\alpha_\ell}] \stackrel{indep}{\sim} N(0, \sigma_{\alpha_\ell}^2), \quad \sigma_{\alpha_\ell} \stackrel{iid}{\sim} C^+(0, 1), \quad p(\sigma_\epsilon^2) \propto 1/\sigma_\epsilon^2, \quad (13)$$

and the SFFM hyperparameters  $a_1 = 5$ ,  $a_2 = 25$ , and  $v_0 = 0.001$ , with an upper bound  $K = 10$  on the number of nonparametric factors. Sensitivity analyses were conducted for  $(a_1, a_2) \in \{(5, 25), (5, 50), (10, 30)\}$  and  $v_0 \in \{0.01, 0.005, 0.00025\}$ . The results for point and interval predictions and estimates of  $\mathbf{Y}_i^*$  and  $\{\alpha_{\ell,i}^*\}$  are highly robust to these hyperparameters. Inference on  $K^*$  is typically robust with the exception of  $v_0 = 0.00025$ , for which the posterior of  $K^*$  becomes more sensitive to  $(a_1, a_2)$ . Hence, we select a larger value of  $v_0$ .

We evaluate point and interval prediction accuracy in Figure 3. Point prediction is evaluated using root mean squared prediction error for  $\mathbf{Y}_i^*$  based on the posterior expectation of  $Y_i$  in (1). Prediction intervals  $(y_i^{(L)}(\tau_j), y_i^{(U)}(\tau_j))$  are estimated using sample quantiles from the relevant posterior predictive draws and evaluated using the mean prediction interval widths  $(nm)^{-1} \sum_{i=1}^n \sum_{j=1}^m \{y_i^{(U)}(\tau_j) - y_i^{(L)}(\tau_j)\}$  and empirical coverage

$(nm)^{-1} \sum_{i=1}^n \sum_{j=1}^m \mathbb{I}\{y_i^*(\tau_j) \in (y_i^{(L)}(\tau_j), y_i^{(U)}(\tau_j))\}$ , where  $\mathbf{y}_i^* = (y_i^*(\tau_1), \dots, y_i^*(\tau_m))'$  is distributed identically to  $\mathbf{y}_i$ . The point predictions all perform similarly when the parametric model is correct ( $K_{true} = 0$ ), yet the PFFM accuracy deteriorates significantly for  $K_{true} > 0$ . The corrections offered by the PFFM-gp provide some improvements, but the SFFMs are far more accurate when  $K_{true} > 0$ . For interval prediction, all models achieve the nominal 95% coverage, yet the SFFMs provide substantially more narrow intervals—and therefore more precise predictive uncertainty quantification—when  $K_{true} > 0$ . The results for interval estimation of  $\{\alpha_{\ell,i}^*\}$  are nearly identical (see the supplementary material) and demonstrate clear advantages for the SFFM when the inferential target is the parametric coefficients.

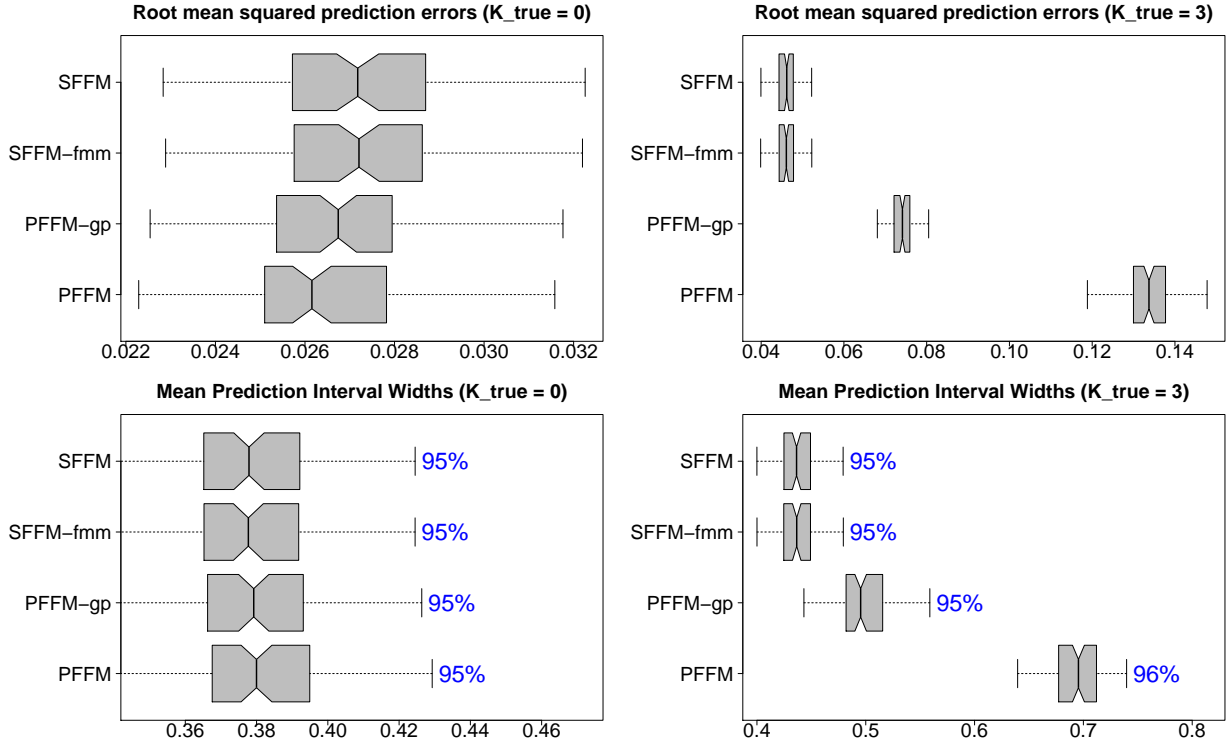


Figure 3: Root mean squared prediction errors for  $Y^*$  (top) and mean credible intervals widths and empirical coverage (bottom) for  $K_{true} = 0$  (left) and  $K_{true} = 3$  (right). The point and interval predictions perform similarly when  $K_{true} = 0$ , but the SFFM offers substantial gains in accuracy and precision when  $K_{true} > 0$ . Results for  $K_{true} = 1$  (omitted) are similar to those for  $K_{true} = 3$ .

We also study the posterior distribution of  $K^* = \sum_{k=1}^K \mathbb{I}\{z_k > k\}$  for estimating  $K_{true}$



and quantifying the necessity of the nonparametric terms. Figure 4 compares the quality of  $\mathbb{P}(K^*|\mathbf{y})$  for the SFFM and the finite mixture alternative. Notably, the ordered spike-and-slab prior results in much larger probabilities on the true rank  $K_{true}$  and substantially better ranked probability scores for the distribution  $\mathbb{P}(K^*|\mathbf{y})$ . Despite fixing  $\kappa = 1$ , the SFFM-fmm repeatedly overestimates the ranks: the simulation average of  $\mathbb{P}(K^* > K_{true}|\mathbf{y})$  is 0.30 for  $K_{true} = 0$ , 0.23 for  $K_{true} = 3$ , and 0.22 for  $K_{true} = 8$ , while the comparable values for the SFFM are 0.15, 0.16, and 0.15, respectively. Hence, the finite mixture alternative introduces unnecessary parameters and relays deceptively strong evidence for additional nonparametric terms. Despite the similar point and interval prediction results for SFFM and SFFM-fmm, the proposed ordered spike-and-slab prior is highly valuable for better rank selection and inference.

Additional simulation results in the supplement include  $K_{true} = 8$ , the Nelson-Siegel template, and further assessments of nonparametric detection via  $\mathbb{P}(K^* > 0|\mathbf{y})$ .

## 6 Applications

### 6.1 Pinch force data

Human motor control is a critical area of research with implications for human physiology, monitoring and mitigating muscle degeneration, and designing robotic devices. Motor control data are often recorded at high resolutions and can be modeled as functional data. Important examples include thumb and forefinger pinching (Ramsay et al., 1995), handwriting analysis (Ramsay, 2000), and reaching motions to study the effects of stroke (Goldsmith and Kitago, 2016). In such applications, human physiology and the laws of motion often dictate a parametric model, which is crucial for understanding the underlying process. However, these parametric models may not adequately describe the observed data, which fundamentally undermines the interpretability of the key parameters of interest.

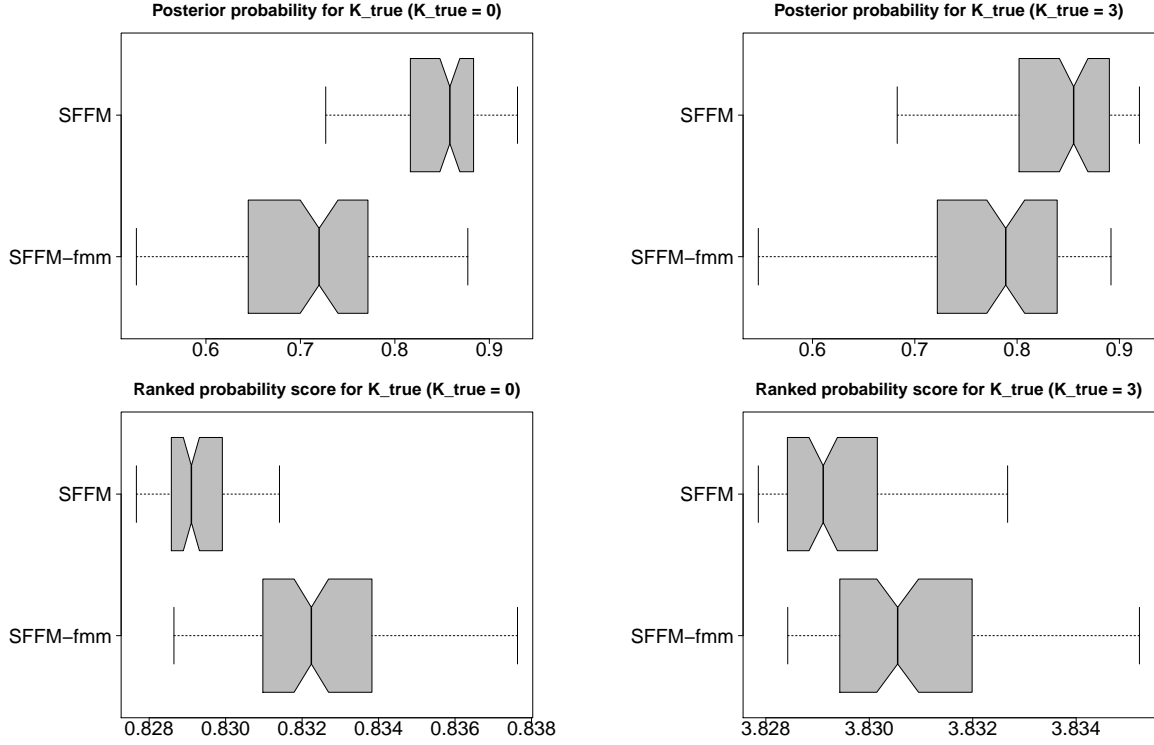


Figure 4: Positively-oriented probability score  $\mathbb{P}(K^* = K_{true}|\mathbf{y})$  (top) and negatively-oriented ranked probability score for  $\mathbb{P}(K^*|\mathbf{y})$  (bottom) for  $K_{true} = 0$  (left) and  $K_{true} = 3$  (right). The proposed ordered spike-and-slab prior provides better rank selection and inference than the finite mixture alternative. Results for  $K_{true} = 1$  (omitted) are similar to those for  $K_{true} = 3$ .

We analyze human pinching data from Ramsay et al. (1995), which reports the force measured by pinching the thumb and forefinger on opposing sides of a 6 cm force meter. The subject was instructed to maintain a background level of constant force, then increase the pinching force to a predetermined maximum level, and finally return to the original background level of constant force. We use data from the `fda` package in R, which consists of  $n = 20$  replicate force curves over time each with  $m = 151$  observations selected such that the maximum of each curve occurred at 0.076 seconds. An example curve is in Figure 1.

To model the pinch force over time  $\tau$ , we adapt a parametric model from Ramsay et al. (1995):

$$g_1(\tau; \gamma_i) = 1, \quad g_2(\tau; \gamma_i) = \exp[-(\log \tau - c_i)^2 / \{2 \exp(\gamma_i)\}], \quad (14)$$

where  $\exp(c_i)$  is the time of the maximum force and  $\gamma_i \in \mathbb{R}$  is a shape parameter. Ramsay et al. (1995) argue that the unnormalized log-normal density  $g_2$  matches the shape of the observed data and offers plausible scientific explanations. For computational convenience, we estimate  $c_i$  as in Ramsay et al. (1995) by fitting a quadratic regression in  $\log(\tau)$  for the response variable  $\log(\mathbf{y}_i)$  restricted to observations  $y_i(\tau) > 0.5$ . The estimate of each  $c_i$  can be recovered from the estimated regression coefficients and is subsequently treated as fixed.

Both PFFMs and SFFMs were fit to the data using the template (14). For partial pooling among subjects, we specify a hierarchical prior on the shape parameters:  $\gamma_i \stackrel{iid}{\sim} N(\mu_\gamma, \sigma_\gamma^2)$ ,  $\mu_\gamma \sim N(0, 10)$ , and  $\sigma_\gamma \sim C^+(0, 1)$ , with the priors from (13) on the remaining parameters. Since the nonlinear parameters  $\gamma_i$  are curve-specific, we construct each  $\mathbf{G}_{\gamma_i}$  for  $i = 1, \dots, n$  using a QR decomposition as in Section 3.2 and modify the orthogonality constraint to be  $\bar{\mathbf{G}}' \mathbf{F} = \mathbf{0}_{L \times K}$  for  $\bar{\mathbf{G}} = n^{-1} \sum_{i=1}^n \mathbf{G}_{\gamma_i}$ . This constraint no longer preserves the posterior factorization of Corollary 2, but nonetheless maintains the crucial distinctness between the parametric and nonparametric terms. For both models, we retain 10000 MCMC samples after discarding 5000 iterations as a burn-in. Traceplots of  $\{Y_i\}$ ,  $\{\alpha_{\ell,i}\}$ , and  $K^*$  (not shown) demonstrate excellent mixing and suggest convergence. The SFFM hyperparameters are set to  $a_1 = 5$ ,  $a_2 = 25$ ,  $v_0 = 0.001$ , and  $K = 10$  as in Section 5.

An example of the fitted values with 95% simultaneous prediction bands for the PFFM and SFFM is in Figure 1. Although the PFFM captures the general shape of the data, it suffers from clear bias around the peak and produces unnecessarily wide prediction bands. The SFFM corrects both issues: the bias is removed and the prediction bands are more precise. Notably, the fitted SFFM curve preserves the same general shape as the PFFM and avoids overfitting despite the increase in modeling complexity.

Posterior uncertainty quantification is also more precise under the SFFM for the parametric factors  $\{\alpha_{\ell,i}\}$ . Figure 5 presents the posterior standard deviations of  $\{\alpha_{\ell,i}\}_{i=1}^n$  for each  $\ell = 1, \dots, L$  under the PFFM and SFFM. Although the posterior expectations (not shown)

are similar, the posterior standard deviations are substantially smaller under the SFFM. For model (14), the linear coefficients  $\{\alpha_{\ell,i}\}$  determine the maximum of the force curve, which is the most prominent feature in the data. The SFFM provides more precise posterior inference for these key parametric factors.

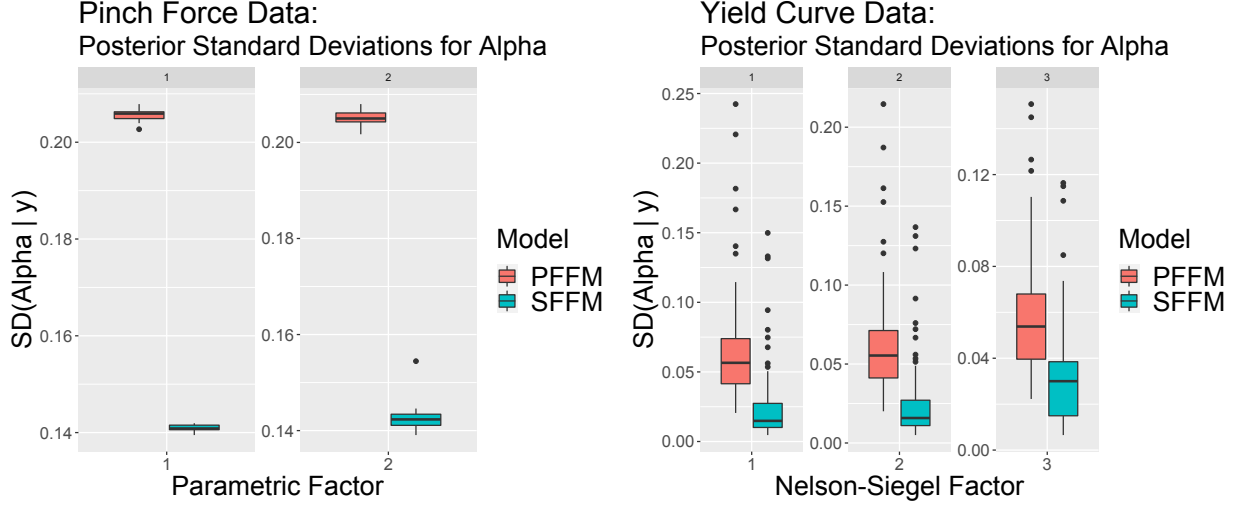


Figure 5: Posterior standard deviations of  $\{\alpha_{\ell,i}\}_{i=1}^n$  for  $\ell = 1, \dots, L$  in the parametric (PFFM) and semiparametric functional factor model (SFFM) for the pinch force data (left) and yield curve data (right). There is a clear and consistent reduction in posterior uncertainty from the PFFM to the SFFM for these key parametric factors.

Additional evidence in favor of the SFFM is presented in Table 2, which estimates the posterior distribution of the effective number of nonparametric terms  $K^*$ . Clearly, there is substantially posterior probability for at least two nonparametric terms, with limited evidence that more than three terms are needed. WAIC similarly favors the SFFM: the estimates are  $-922$  and  $-3007$  for the PFFM and SFFM, respectively.

$k$	0	1	2	3	4	5	$\geq 6$
$\mathbb{P}(K^* = k   \mathbf{y})$	0.003	0.147	0.707	0.135	0.007	0.001	0

Table 2: Posterior probabilities  $\mathbb{P}(K^* = k | \mathbf{y})$  for the pinch force data. There is strong evidence for a nonparametric component.

## 6.2 Dynamic yield curves

Yield curves play a fundamental role in economic and financial analyses: they provide essential information about current and future economic conditions, including inflation, business cycles, and monetary policies, and are used to price fixed-income securities and construct forward curves. The yield curve  $Y_i(\tau)$  describes how interest rates vary as a function of the length of the borrowing period, or time to maturity  $\tau$ , at each time  $i$ . Naturally, yield curves can be modeled as functional data that evolve dynamically over time.

Yield curve models most commonly employ the parametric Nelson-Siegel basis (Nelson and Siegel, 1987):

$$g_1(\tau; \gamma) = 1, \quad g_2(\tau; \gamma) = \{1 - \exp(-\tau\gamma)\}/(\tau\gamma), \quad g_3(\tau; \gamma) = g_2(\tau; \gamma) - \exp(-\tau\gamma) \quad (15)$$

where  $g_1$  is the *level*,  $g_2$  is the *slope*, and  $g_3$  is the *curvature*. The nonlinear parameter  $\gamma > 0$  is commonly treated as fixed, such as  $\gamma = 0.0609$  (Diebold and Li, 2006), but otherwise may be estimated. We use a weakly informative Gamma prior for  $\gamma$  with prior mean 0.0609 and prior variance 0.5. Both the PFFM and the SFFM with this prior on  $\gamma$  are favored by WAIC over their respective counterparts with fixed  $\gamma = 0.0609$ .

To capture the yield curve dynamics, we model the parametric Nelson-Siegel factors as an AR(1):

$$\alpha_{\ell,i} = \mu_\ell + \phi_\ell(\alpha_{\ell,i-1} - \mu_\ell) + \zeta_{\ell,i}, \quad \zeta_{\ell,i} \stackrel{indep}{\sim} N(0, \sigma_{\zeta_\ell}^2). \quad (16)$$

The PFFM with (15) and (16) is also known as the *dynamic Nelson-Siegel model* (Diebold and Li, 2006). The dynamic Nelson-Siegel factors  $\{\alpha_{\ell,i}\}$  may be viewed as the state variables in a dynamic linear model. Importantly, the orthogonality constraints on  $\{g_\ell\}$  and  $\{f_k\}$  admit a convenient and low-dimensional state simulation algorithm for efficient joint sampling of the dynamic factors  $\{\alpha_{\ell,i}\}$ ; see the supplementary material for details.

The dynamic model (16) is accompanied by a diffuse prior  $\mu_\ell \stackrel{iid}{\sim} N(0, 10^6)$  and a weakly informative prior  $(\phi_\ell + 1)/2 \stackrel{iid}{\sim} \text{Beta}(5, 2)$ —which ensures stationarity of the dynamic factors  $\{\alpha_{\ell,i}\}$  and therefore  $\{Y_i\}$  and  $\{\mathbf{y}_i\}$ —along with  $\sigma_{\zeta_\ell} \stackrel{iid}{\sim} C^+(0, 1)$  for  $\ell = 1, \dots, L$ . In addition, we generalize (2) to accommodate stochastic volatility in the observation error variance,  $\epsilon_{i,j} \stackrel{indep}{\sim} N(0, \sigma_{\epsilon_i}^2)$ , with  $\log \sigma_{\epsilon_i}^2 \sim \text{AR}(1)$ , which is an essential component in many economic and financial models (Kim et al., 1998). For these AR(1) parameters, we adopt the priors and sampling algorithm from Kowal (2020).

We evaluate the suitability of the Nelson-Siegel basis for modeling monthly unsmoothed Fama-Bliss US government bond yields from 2000-2009 ( $n = 120$ ) provided by Van Dijk et al. (2014). These data are available for maturities of 3, 6, 9, 12, 15, 18, 21, 24, 30, 36, 48, 60, 72, 84, 96, 108 and 120 months ( $m = 17$ ). The inferential targets are the latent curves  $Y_i$ , the dynamic Nelson-Siegel factors  $\{\alpha_{i,\ell}\}$ , and the effective number of nonparametric terms  $K^*$ . The SFFM hyperparameter and MCMC specifications from Section 6.1 are adopted here, again with excellent mixing and convergence for these key parameters.

Figure 1 shows the PFFM and SFFM fitted values with 95% simultaneous prediction bands for the yield curve in September 2008 during the onset of the Great Recession. The PFFM produces a reasonable shape for the yield curve, yet—as with the pinch force data—suffers from clear bias and overconservative prediction bands. The SFFM corrects these deficiencies without distorting the general shape of the curve or overfitting to the data.

Similar results are obtained in Figure 5 for the dynamic Nelson-Siegel factors. The SFFM offers substantial reductions in posterior standard deviation for all three dynamic Nelson-Siegel factors. These factors are fundamental for describing the shape of the yield curve; reducing the posterior uncertainty is a crucial advantage of the SFFM. Importantly, the simulation study confirms that the reduced posterior uncertainty quantification from the SFFM nonetheless retains valid calibration, or more specifically, correct nominal coverage of the posterior credible intervals.

We summarize the posterior distribution  $\mathbb{P}(K^*|\mathbf{y})$  of the effective number of nonparametric terms in Table 3. The evidence for the nonparametric factors is moderate: we estimate  $\mathbb{P}(K^* > 0|\mathbf{y}) = 0.09$ .

$k$	0	1	2	$\geq 3$
$\mathbb{P}(K^* = k \mathbf{y})$	0.910	0.087	0.003	0

Table 3: Posterior probabilities  $\mathbb{P}(K^* = k|\mathbf{y})$  for the yield curve data. There is moderate evidence for a nonparametric component.

There are other compelling reasons to include the nonparametric factors in a dynamic Nelson-Siegel model. First, the uncertainty quantification for  $\{Y_i\}$  and  $\{\alpha_{\ell,i}\}$  is more precise in the SFFM than in the PFFM (see Figures 1 and 5). Second, WAIC decisively prefers the SFFM (-10229) over the PFFM (-5516), which suggests potential improvements in out-of-sample predictive capabilities. Third, the additional computational burdens of the SFFM are minimal. Due to the orthogonality constraints, the sampling steps for  $\{\alpha_{\ell,i}\}$  and associated parameters are identical for the PFFM and the SFFM, which permits full and robust model development for the parametric factors. The computational cost associated with sampling the nonparametric terms is small: the computing time per 1000 iterations is 21s and 23s for the PFFM and SFFM, respectively (using R on a MacBook Pro, 2.8 GHz Intel Core i7).

## 7 Discussion

We proposed a Bayesian model for semiparametric functional data analysis. The model augments a parametric template with an infinite-dimensional nonparametric functional basis. Crucially, the nonparametric component is regularized with an ordered spike-and-slab prior, which implicitly provides rank selection for infinite-dimensional models and satisfies appealing theoretical properties. This prior is accompanied by a parameter expansion scheme customized to boost MCMC efficiency, and is broadly applicable for Bayesian (functional, spatial, and temporal) factor models. The nonparametric basis functions are learned from

the data but constrained to be orthogonal to the parametric basis functions, which preserves distinctness between the parametric and nonparametric components and offers key computational simplifications. Our analyses of synthetic data, human motor control data, and dynamic interest rates demonstrate clear advantages of the semiparametric modeling framework relative to parametric alternatives. The proposed approach eliminates bias, reduces excessive posterior and predictive uncertainty, and provides reliable inference on the effective number of nonparametric terms—all with minimal additional computational costs.

There are several promising extensions that remain for future work. First, formulation of the parametric template in (1) can be generalized, for example to include a functional regression term with scalar or functional covariates. Second, the ordered spike-and-slab prior currently uses independent and identically distributed variables in the parameter expansion (11). Adaptations to include dependence among these variables, such as regression models, clustering, and spatio-temporal dependence, would broaden the applicability of the prior. Lastly, we studied only a small subset of many possible parametric templates. For applications that rely on such parametric models, the proposed semiparametric modeling framework can directly assess the adequacy of these models—and perhaps suggest improvements.

## Acknowledgements

Research was sponsored by the Army Research Office and was accomplished under Grant Number W911NF-20-1-0184 (Kowal). The views and conclusions contained in this document are those of the authors and should not be interpreted as representing the official policies, either expressed or implied, of the Army Research Office or the U.S. Government. The U.S. Government is authorized to reproduce and distribute reprints for Government purposes notwithstanding any copyright notation herein.



## References

- Bhattacharya, A. and Dunson, D. B. (2011). Sparse Bayesian infinite factor models. *Biometrika*, 98(2):291–306.
- Bianchi, F., Mumtaz, H., and Surico, P. (2009). The great moderation of the term structure of UK interest rates. *Journal of Monetary Economics*, 56(6):856–871.
- Canale, A., Lijoi, A., Nipoti, B., and Prünster, I. (2017). On the Pitman-Yor process with spike and slab base measure. *Biometrika*, 104(3):681–697.
- Castillo, I. and van der Vaart, A. (2012). Needles and straw in a haystack: Posterior concentration for possibly sparse sequences. *The Annals of Statistics*, 40(4):2069–2101.
- Chen, S. T., Xiao, L., and Staicu, A.-M. (2019). Model Testing for Generalized Scalar-on-Function Linear Models. *arXiv preprint arXiv:1906.04889*.
- Diebold, F. X. and Li, C. (2006). Forecasting the term structure of government bond yields. *Journal of Econometrics*, 130(2):337–364.
- Durante, D. (2017). A note on the multiplicative gamma process. *Statistics and Probability Letters*, 122:198–204.
- Durbin, J. and Koopman, S. J. (2002). A simple and efficient simulation smoother for state space time series analysis. *Biometrika*, 89(3):603–615.
- Gelman, A. (2006). Prior distributions for variance parameters in hierarchical models. *Bayesian Analysis*, 1(3):515–534.
- Goldsmith, J. and Kitago, T. (2016). Assessing systematic effects of stroke on motor control by using hierarchical function-on-scalar regression. *Journal of the Royal Statistical Society. Series C: Applied Statistics*, 65(2):215–236.
- Griffiths, T. L. and Ghahramani, Z. (2011). The Indian buffet process: An introduction and review. *Journal of Machine Learning Research*, 12(4).
- Heckman, N. E. and Ramsay, J. O. (2000). Penalized regression with model-based penalties. *Canadian Journal of Statistics*, 28(2):241–258.
- Ishwaran, H. and James, L. F. (2001). Gibbs sampling methods for stick-breaking priors. *Journal of the American Statistical Association*, 96(453):161–173.

- Ishwaran, H. and Rao, J. S. (2005). Spike and slab variable selection: Frequentist and Bayesian strategies. *Annals of Statistics*, 33(2):730–773.
- Kim, S., Shephard, N., and Chib, S. (1998). Stochastic Volatility: Likelihood Inference and Comparison with ARCH Models. *Review of Economic Studies*, 65(3):361–393.
- Kowal, D. R. (2020). Dynamic Regression Models for Time-Ordered Functional Data. *Bayesian Analysis*.
- Kowal, D. R. and Bourgeois, D. C. (2020). Bayesian Function-on-Scalars Regression for High-Dimensional Data. *Journal of Computational and Graphical Statistics*, 29(3):1–10.
- Lee, W., Miranda, M. F., Rausch, P., Baladandayuthapani, V., Fazio, M., Downs, J. C., and Morris, J. S. (2018). Bayesian semiparametric functional mixed models for serially correlated functional data, with application to glaucoma data. *Journal of the American Statistical Association*.
- Legramanti, S., Durante, D., and Dunson, D. B. (2020). Bayesian cumulative shrinkage for infinite factorizations. *Biometrika*, 107(3):745–752.
- Mikulich, S. K., Zerbe, G. O., Jones, R. H., and Crowley, T. J. (2003). Comparing linear and nonlinear mixed model approaches to cosinor analysis. *Statistics in Medicine*, 22(20):3195–3211.
- Molenberghs, G. and Verbeke, G. (2000). *Linear mixed models for longitudinal data*. Springer.
- Neal, R. M. (2003). Slice sampling. *Annals of Statistics*, pages 705–741.
- Nelson, C. R. and Siegel, A. F. (1987). Parsimonious Modeling of Yield Curves. *The Journal of Business*, 60(4):473.
- Ohn, I. and Kim, Y. (2021). Posterior Consistency of Factor Dimensionality in High-Dimensional Sparse Factor Models. *Bayesian Analysis*, 1(1):1–24.
- Rai, P. and Daumé III, H. (2009). The infinite hierarchical factor regression model. In Koller, D., Schuurmans, D., Bengio, Y., and Bottou, L., editors, *Advances in neural information processing systems*. Curran Associates, Inc.

- Ramsay, J. O. (2000). Functional components of variation in handwriting. *Journal of the American Statistical Association*, 95(449):9–15.
- Ramsay, J. O. and Dalzell, C. J. (1991). Some tools for functional data analysis. *Journal of the Royal Statistical Society: Series B (Methodological)*, 53(3):539–561.
- Ramsay, J. O., Wang, X., and Flanagan, R. (1995). A functional data analysis of the pinch force of human fingers. *Journal of the Royal Statistical Society: Series C (Applied Statistics)*, 44(1):17–30.
- Rockova, V. (2018). Bayesian estimation of sparse signals with a continuous spike and slab prior. *The Annals of Statistics*, 46(1):401–437.
- Ročková, V. and George, E. I. (2016). Fast Bayesian factor analysis via automatic rotations to sparsity. *Journal of the American Statistical Association*, 111(516):1608–1622.
- Sang, P., Wang, L., and Cao, J. (2017). Parametric functional principal component analysis. *Biometrics*, 73(3):802–810.
- Scarpa, B. and Dunson, D. B. (2009). Bayesian hierarchical functional data analysis via contaminated informative priors. *Biometrics*, 65(3):772–780.
- Scarpa, B. and Dunson, D. B. (2014). Enriched stick-breaking processes for functional data. *Journal of the American Statistical Association*, 109(506):647–660.
- Scheipl, F., Fahrmeir, L., and Kneib, T. (2012). Spike-and-slab priors for function selection in structured additive regression models. *Journal of the American Statistical Association*, 107(500):1518–1532.
- Teh, Y. W., Grür, D., and Ghahramani, Z. (2007). Stick-breaking construction for the Indian buffet process. In *Artificial Intelligence and Statistics*, pages 556–563. PMLR.
- Van Dijk, D., Koopman, S. J., der Wel, M., and Wright, J. H. (2014). Forecasting interest rates with shifting endpoints. *Journal of Applied Econometrics*, 29(5):693–712.
- Wagner, A. B., Hill, E. L., Ryan, S. E., Sun, Z., Deng, G., Bhadane, S., Martinez, V. H., Wu, P., Li, D., Anand, A., Acharya, J., and Matteson, D. S. (2020). Social Distancing Has Merely Stabilized COVID-19 in the US. *Stat*, page e302.

- Wand, M. P., Ormerod, J. T., Padoan, S. A., and Frührwirth, R. (2011). Mean field variational Bayes for elaborate distributions. *Bayesian Analysis*, 6(4):847–900.
- Wang, Y. (2011). *Smoothing Splines: Methods and Applications*. CRC Press.
- Welham, S. J., Cullis, B. R., Kenward, M. G., and Thompson, R. (2006). The analysis of longitudinal data using mixed model L-splines. *Biometrics*, 62(2):392–401.
- Wood, S. (2006). *Generalized additive models: an introduction with R*. CRC press.

## A Proofs

**Proposition 5.** For  $\varepsilon > 0$  and fixed  $\theta_0$ , let  $\mathbb{B}_\varepsilon(\theta_0) = \{\theta_k : |\theta_k - \theta_0| < \varepsilon\}$ . Prior (3)-(4) implies that  $\mathbb{P}(|\theta_k - \theta_0| \leq \varepsilon) < \mathbb{P}(|\theta_{k+1} - \theta_0| \leq \varepsilon)$  whenever  $P_{slab}\{\mathbb{B}_\varepsilon(\theta_0)\} < P_{spike}\{\mathbb{B}_\varepsilon(\theta_0)\}$ .

*Proof.* The proof proceeds directly:

$$\begin{aligned} \mathbb{P}(|\theta_k - \theta_0| \leq \varepsilon) &= \mathbb{E}[P_k\{\mathbb{B}_\varepsilon(\theta_0)\}] = \mathbb{E}[(1 - \pi_k)P_{slab}\{\mathbb{B}_\varepsilon(\theta_0)\} + \pi_k P_{spike}\{\mathbb{B}_\varepsilon(\theta_0)\}] \\ &= \mathbb{E}\{(1 - \pi_k)\}P_{slab}\{\mathbb{B}_\varepsilon(\theta_0)\} + \mathbb{E}(\pi_k)P_{spike}\{\mathbb{B}_\varepsilon(\theta_0)\} \\ &= P_{slab}\{\mathbb{B}_\varepsilon(\theta_0)\}\{\kappa/(1 + \kappa)\}^k + P_{spike}\{\mathbb{B}_\varepsilon(\theta_0)\}[1 - \{\kappa/(1 + \kappa)\}^k] \\ &= P_{spike}\{\mathbb{B}_\varepsilon(\theta_0)\} + \{\kappa/(1 + \kappa)\}^k[P_{slab}\{\mathbb{B}_\varepsilon(\theta_0)\} - P_{spike}\{\mathbb{B}_\varepsilon(\theta_0)\}] \end{aligned}$$

noting  $\mathbb{E}(\pi_k) = 1 - \{\iota\kappa/(\iota + \kappa)\}^k = 1 - \{\kappa/(1 + \kappa)\}^k$ . Since  $\{\kappa/(1 + \kappa)\}^k \in [0, 1]$  is decreasing in  $k$  and the remaining terms are invariant to  $k$ , the result follows.  $\square$

**Proposition 6.** Let  $\theta^{(K)} = \{\theta_k\}_{k=1}^K$  denote the sequence  $\{\theta_k\}_{k=1}^\infty$  truncated at  $K$ . For  $0 < v_0 < \varepsilon < 1$ , we have  $\mathbb{P}\{d_\infty(\theta, \theta^{(K)}) > \varepsilon\} \leq \kappa\{\kappa/(1 + \kappa)\}^K$ .

*Proof.* For the prior (5), note that  $P_{slab} = \delta_1$  and  $P_{spike} = \delta_{v_0}$ , so  $P_{slab}\{\bar{\mathbb{B}}_\varepsilon(0)\} = 1$  if  $\varepsilon < 1$  and  $P_{spike}\{\bar{\mathbb{B}}_\varepsilon(0)\} = 0$  if  $\varepsilon > v_0$ , where  $\bar{\mathbb{B}}_\varepsilon(0)$  denotes the complement of  $\mathbb{B}_\varepsilon(0)$ . Using the proof of Proposition 1, we have  $\mathbb{P}\{d_\infty(\theta, \theta^{(K)}) > \varepsilon\} = \mathbb{P}\{\sup_{k>K} |\theta_k| > \varepsilon\} \leq \sum_{k>K} \mathbb{P}(|\theta_k| > \varepsilon) = \sum_{k>K} \{\kappa/(1 + \kappa)\}^k = \kappa\{\kappa/(1 + \kappa)\}^K$ .  $\square$

**Proposition 7.** The CUSP (4) satisfies  $(1 - \pi_k) = \mu_{(k)}$  where  $\mu_{(1)} > \dots > \mu_{(K)}$  are the ordered (slab) probabilities from the stick-breaking construction (8) of the IBP (7).

*Proof.* Let  $\nu'_\ell = (1 - \nu_\ell) \stackrel{iid}{\sim} \text{Beta}(\iota\kappa, \iota)$ , so  $\omega_h = (1 - \nu'_h) \prod_{\ell=1}^{h-1} \nu'_\ell = \prod_{\ell=1}^{h-1} \nu'_\ell - \prod_{\ell=1}^h \nu'_\ell$ . By cancelling terms in the cumulative summation  $\pi_k = \sum_{h=1}^k \omega_h$ , the result for  $1 - \pi_k$  follows.  $\square$

**Lemma 3.** Let  $\ell_n < \varepsilon_n < 1$  with  $\ell_n = (\kappa/(\kappa + 1))^{K_{0n}}$ . For the CUSP prior (3)-(4) and a positive constant  $C > 1$ , the remainder term  $R_n = \sum_{k \geq K_{0n}} \omega_k$  satisfies

$$\mathbb{P}(R_n > \varepsilon_n) \leq \exp\{-CK_{0n}\}. \quad (\text{A.1})$$

*Proof.* Rewriting the remainder as  $R_n = \prod_{h=1}^{K_{0n}} (1 - \nu_h)$ , the *a priori* expectation of the remainder is

$$\mathbb{E}(R_n) = \prod_{h=1}^{K_{0n}} \mathbb{E}(1 - \nu_h) = \left(\frac{\kappa}{\kappa + 1}\right)^{K_{0n}}$$

from which we conclude that

$$\mathbb{P}(R_{0n} > \varepsilon_n) \leq \frac{1}{\varepsilon_n} \left( \frac{\kappa}{\kappa + 1} \right)^{K_{0n}} \leq \exp\{-CK_{0n}\},$$

where the first inequality follows from Markov's inequality, and the last one from the assumptions on the rate of contraction of  $\varepsilon_n$ .  $\square$

Before proving Theorem 1, we introduce the following lemma:

**Lemma 4.** *Let  $1 < r < \sqrt{n}$ ,  $a_1 > 1/2$ , and  $a_1 \leq a_2$ . Under the CUSP and NMIG in (3)-(4) and (5), respectively, then a priori*

$$\mathbb{P}\left(|\eta_h| < \frac{r}{\sqrt{n}}\right) > \left\{1 - \left(\frac{\kappa}{\kappa + 1}\right)^h\right\} \left(1 - \frac{1}{1 + \frac{a_1 r^2}{nv_0 a_2}}\right)$$

*Proof.* First, we consider the conditional probability

$$\mathbb{P}\left(|\eta_h| < \frac{r}{\sqrt{n}} \mid \pi_h\right)$$

and then integrate  $\pi_h$  with respect to the CUSP. We know that, in a neighborhood of zero, the density function of a Student  $t$  random variable with degrees of freedom greater or equal to 1 is bounded below by the density of a Cauchy random variable. The cumulative distribution function of a Cauchy random variable is

$$F(t) = \frac{1}{2} + \frac{1}{\pi} \arctan(t).$$

Hence, for sufficiently large  $n$  we can write

$$\begin{aligned} \mathbb{P}\left(|\eta_h| < \frac{r}{\sqrt{n}} \mid \pi_h\right) &\geq (1 - \pi_h) \frac{2}{\pi} \arctan\left(\frac{r\sqrt{a_1}}{\sqrt{a_2 n}}\right) + \pi_h \frac{2}{\pi} \arctan\left(\frac{r\sqrt{a_1}}{\sqrt{a_2 n v_0}}\right) \\ &\geq \frac{2\pi_h}{\pi} \arctan\left(\frac{r\sqrt{a_1}}{\sqrt{nv_0 a_2}}\right) \\ &\geq \pi_h \left(1 - \frac{1}{1 + \frac{a_1 r^2}{nv_0 a_2}}\right) \end{aligned}$$

and the last inequality holds since  $2/\pi \arctan(t) > (1 - 1/(1 + t^2))$  for  $t \in (0, 1)$ . Finally,

integrating out  $\pi_h$  yields

$$\mathbb{P} \left( |\eta_h| < \frac{r}{\sqrt{n}} \right) \geq \mathbb{E} (\pi_h) \left( 1 - \frac{1}{1 + \frac{a_1 r^2}{n v_0 a_2}} \right) = \left\{ 1 - \left( \frac{\kappa}{\kappa + 1} \right)^h \right\} \left( 1 - \frac{1}{1 + \frac{a_1 r^2}{n a_2}} \right).$$

□

**Theorem 2.** *Let  $\ell_n < \varepsilon_n < 1$  with  $\ell_n = (\kappa/(\kappa + 1))^{K_{0n}}$  and assume (C1)-(C3) and  $C > 2Ae$ . For the CUSP and NMIG priors, (3)-(4) and (5), respectively, the posterior satisfies  $\lim_{n \rightarrow \infty} \mathbb{E}_0 \{ \mathbb{P} (R_n > \varepsilon_n \mid y_1, \dots, y_n) \} = 0$ .*

*Proof.* Let  $y^{(n)} = (y_1, \dots, y_n)'$  denote the observed data. For  $\eta \in \mathbb{R}^n$ , let  $f_\eta(\cdot)$  denote the probability density function of a  $N(\eta, I_n)$  distribution and  $f_{\eta_i}(\cdot)$  denote the related univariate marginal. Let  $f_0(\cdot)$  be the true density, i.e., a Gaussian distribution with mean  $\eta_0$  and identity covariance. Recall that  $\eta_{0i} \neq 0$  for  $i \leq K_{0n}$  while the remaining  $\eta_{0i}$  for  $i > K_{0n}$  are all null. Let  $\Pi(\cdot)$  the CUSP prior measure on the  $\eta$  parameters. Let  $E_n$  be the target event,

$$E_n = \{R_{K_n} > \varepsilon_n\}.$$

Following Castillo and van der Vaart (2012) and Rockova (2018), we write

$$\mathbb{P} (E_n \mid y^{(n)}) = \frac{\int_{E_n} \prod_{i=1}^n \frac{f_{\eta_i}(y_i)}{f_{0i}(y_i)} d\Pi(\eta_i)}{\int \prod_{i=1}^n \frac{f_{\eta_i}(y_i)}{f_{0i}(y_i)} d\Pi(\eta_i)} = \frac{N_n}{D_n}. \quad (\text{A.2})$$

We introduce an event  $A_n$  with large probability under the true data generating process. Specifically, let  $R = \{h = K_{n0} + 1, \dots, n\}$  and define

$$A_n := \{D_n \geq e^{r_n^2} \mathbb{P}(\|\eta_R\| \leq r_n)\}.$$

If we decompose the probability in (A.2) in the sum of two complementary conditional probabilities (conditioning on  $A_n$  and its complement  $A_n^c$ ) we can write

$$\mathbb{E}_0 [\mathbb{P} (E_n \mid y^{(n)})] \leq \mathbb{E}_0 [\mathbb{P} (E_n \mid y^{(n)}) \mathbb{I}_{A_n}] + \mathbb{P}_0(A_n^c)$$

Now thanks to Lemma 5.2 of Castillo and van der Vaart (2012) the second summand has negligible probability for increasing  $n$ :  $\mathbb{P}_0(A_n^c) \leq \exp\{-r_n^2\}$ . Applying (A.2), we have

$$\mathbb{E}_0 [\mathbb{P} (E_n \mid y^{(n)})] \leq \frac{\mathbb{P}(E_n)}{e^{-r_n^2} \mathbb{P}(\|\eta_R\| \leq r_n)} + \exp\{-r_n^2\},$$

where  $\mathbb{P}(E_n)$  is simply the prior probability. We can now use Lemma 3 to bound the numerator and Lemma 4 to bound the denominator. Specifically, we have  $\mathbb{P}(\|\eta\| \leq r_n) \geq \mathbb{P}(|\eta_{K_{0n}}| \leq r_n/\sqrt{n})^{n-K_{n0}}$  and hence, Lemma 4 yields

$$\mathbb{P}(\|\eta_R\| \leq r_n) \geq \left(1 - \left(\frac{\kappa}{\kappa+1}\right)^{K_{0n}}\right)^{n-K_{n0}} \left(1 - \frac{1}{1 + \frac{a_1 r_n^2}{na_2 v_0}}\right)^{n-K_{n0}}.$$

Now, we have  $\left(\frac{\kappa}{\kappa+1}\right)^{K_{0n}} < AK_{0n}/n$  for high  $n$  and a constant  $A > 1/2$ . Thus, choosing  $r_n^2 = K_{0n}$  and considering (C1), we can write

$$\mathbb{P}(\|\eta_R\| \leq r_n) \geq \left(1 - \frac{AK_{0n}}{n}\right)^n \left(1 - \frac{1}{n}\right)^n \geq \left(\frac{1}{2e}\right)^{AK_{0n}+1},$$

where the last inequality follows from  $(1-x)^{1/x} > 1/(2e)$  for  $0 < x < 0.5$ . Finally, using Lemma 3, we get

$$\mathbb{E}_0 [\mathbb{P}(E_n | y^{(n)})] \leq 2 \exp\{-K_{0n}[C - 1 - A \log(2e)] + 1\} + \exp\{-K_{0n}\}.$$

Then, since  $C > 2Ae > 1 + A \log(2e)$  for  $A > 1/2$ , we conclude  $\mathbb{E}_0\{\mathbb{P}(E_n | y^{(n)})\} \rightarrow 0$ .  $\square$

**Proposition 8.** For  $\varepsilon > 0$ ,  $\mathbb{P}(|\beta_{k,i}| \leq \varepsilon) < \mathbb{P}(|\beta_{k+1,i}| \leq \varepsilon)$  whenever  $v_0 < 1$ .

*Proof.* Since  $\{\xi_{k,i}\}$  are iid (upon marginalization over  $\{m_{\xi_{k,i}}\}$ ), it follows that  $\mathbb{P}(|\beta_{k,i}| \leq \varepsilon) = \mathbb{P}(|\eta_k \xi_{k,i}| \leq \varepsilon) = \mathbb{P}(|\eta_k \xi_{k+1,i}| \leq \varepsilon)$ . Then we proceed directly:

$$\begin{aligned} \mathbb{P}(|\beta_{k,i}| \leq \varepsilon) &= \mathbb{P}(|\eta_k \xi_{k+1,i}| \leq \varepsilon) = \mathbb{E}\{\mathbb{I}(|\eta_k| |\xi_{k+1,i}| \leq \varepsilon)\} \\ &= \mathbb{E}[\mathbb{E}\{\mathbb{I}(|\eta_k| |\xi_{k+1,i}| \leq \varepsilon) | \xi_{k+1,i}\}] \\ &= \mathbb{E}[\mathbb{P}(|\eta_k| |\xi_{k+1,i}| \leq \varepsilon | \xi_{k+1,i})] \\ &< \mathbb{E}[\mathbb{P}(|\eta_{k+1}| |\xi_{k+1,i}| \leq \varepsilon | \xi_{k+1,i})] \\ &= \mathbb{P}(|\beta_{k+1,i}| \leq \varepsilon), \end{aligned}$$

where the inequality follows from Corollary 1.  $\square$

**Lemma 5.** When  $\mathbf{G}'_\gamma \mathbf{F} = \mathbf{0}_{L \times K}$ , the likelihood (14) factorizes:  $p(\mathbf{y} | \gamma, \{\boldsymbol{\alpha}_i\}, \mathbf{F}, \{\boldsymbol{\beta}_i\}, \sigma_\epsilon^2) = p_0(\mathbf{y} | \gamma, \{\boldsymbol{\alpha}_i\}, \sigma_\epsilon^2) p_1(\mathbf{y} | \mathbf{F}, \{\boldsymbol{\beta}_i\}, \sigma_\epsilon^2)$ , where  $p_0$  depends on the parametric terms,  $\gamma$  and  $\{\boldsymbol{\alpha}_i\}$ , and the error variance  $\sigma_\epsilon^2$ , and  $p_1$  depends on the nonparametric terms,  $\mathbf{F}$  and  $\{\boldsymbol{\beta}_i\}$ , and  $\sigma_\epsilon^2$ .

*Proof.* Observing that  $\|\mathbf{y}_i - \mathbf{G}_\gamma \boldsymbol{\alpha}_i - \mathbf{F} \boldsymbol{\beta}_i\|^2 = \|\mathbf{y}_i\|^2 + \|\mathbf{G}_\gamma \boldsymbol{\alpha}_i\|^2 + \|\mathbf{F} \boldsymbol{\beta}_i\|^2 - 2\boldsymbol{\alpha}_i \mathbf{G}'_\gamma \mathbf{y}_i -$



$2\alpha_i \mathbf{G}'_\gamma \mathbf{F} \beta_i - 2\beta_i \mathbf{F}' \mathbf{y}_i = \|\mathbf{y}_i\|^2 + (\|\mathbf{G}_\gamma \alpha_i\|^2 - 2\alpha_i \mathbf{G}'_\gamma \mathbf{y}_i) + (\|\mathbf{F} \beta_i\|^2 - 2\beta_i \mathbf{F}' \mathbf{y}_i)$ , the joint likelihood factorizes into

$$\begin{aligned}
p(\mathbf{y}|-) &= \prod_{i=1}^n p(\mathbf{y}_i|-) = \prod_{i=1}^n (2\pi\sigma_\epsilon^2)^{-m/2} \exp\{-\|\mathbf{y}_i - \mathbf{G}_\gamma \alpha_i - \mathbf{F} \beta_i\|^2 / (2\sigma_\epsilon^2)\} \\
&= \prod_{i=1}^n (2\pi\sigma_\epsilon^2)^{-m/2} \exp[-\{\|\mathbf{y}_i\|^2 + (\|\mathbf{G}_\gamma \alpha_i\|^2 - 2\alpha_i \mathbf{G}'_\gamma \mathbf{y}_i) + (\|\mathbf{F} \beta_i\|^2 - 2\beta_i \mathbf{F}' \mathbf{y}_i)\} / (2\sigma_\epsilon^2)] \\
&= (2\pi\sigma_\epsilon^2)^{-nm/2} \exp\left\{-\sum_{i=1}^n \|\mathbf{y}_i\|^2 / (2\sigma_\epsilon^2)\right\} \exp\left\{-\sum_{i=1}^n (\|\mathbf{G}_\gamma \alpha_i\|^2 - 2\alpha_i \mathbf{G}'_\gamma \mathbf{y}_i) / (2\sigma_\epsilon^2)\right\} \\
&\quad \exp\left\{-\sum_{i=1}^n (\|\mathbf{F} \beta_i\|^2 - 2\beta_i \mathbf{F}' \mathbf{y}_i) / (2\sigma_\epsilon^2)\right\}
\end{aligned}$$

which produces the necessary product factorization. Note that orthonormality of  $\mathbf{G}_\gamma$  and  $\mathbf{F}$  imply additional simplifications, since  $\|\mathbf{G}_\gamma \alpha_i\|^2 = \|\alpha_i\|^2$  and  $\|\mathbf{F} \beta_i\|^2 = \|\beta_i\|^2$ .  $\square$

## B MCMC algorithm

We outline the Gibbs sampling algorithm for the semiparametric functional factor model (SFFM). Specifically, we present full conditional updates for the model with the following priors on the parametric components:

$$[\alpha_{\ell,i} | \sigma_{\alpha_\ell}] \stackrel{indep}{\sim} N(0, \sigma_{\alpha_\ell}^2), \quad \sigma_{\alpha_\ell} \stackrel{iid}{\sim} C^+(0, 1), \quad p(\sigma_\epsilon^2) \propto 1/\sigma_\epsilon^2,$$

and assume a generic prior  $p(\gamma)$  for the nonlinear parameter  $\gamma$  (if unknown). Naturally, the sampling step for  $\gamma$  is omitted if there are no unknown nonlinear parameters.

### Gibbs sampling algorithm:

1. **Imputation:** for any unobserved  $\tau^*$  for functional observation  $i$ , sample

$$[y_i(\tau^*) | -] \stackrel{indep}{\sim} N\left(\sum_{\ell=1}^L g_\ell(\tau^*; \gamma) \alpha_{\ell,i} + \sum_{k=1}^K f_k(\tau^*) \beta_{k,i}, \sigma_\epsilon^2\right);$$

2. **Nonlinear parameter:** if  $\gamma$  is unknown, sample

$$p(\gamma|-) \propto p(\gamma) \exp\left(-\frac{1}{2} \sum_{i=1}^n \|\mathbf{y}_i - \mathbf{G}_\gamma \boldsymbol{\alpha}_i - \mathbf{F} \boldsymbol{\beta}_i\|^2 / \sigma_\epsilon^2\right)$$

using a slice sampler (Neal, 2003);

3. **Nonparametric parameters:** for  $k = 1, \dots, K$  (in random order),

(a) Sample the unconstrained coefficients

$$\boldsymbol{\psi}_k^0 \sim N(\mathbf{Q}_{\boldsymbol{\psi}_k}^{-1} \boldsymbol{\ell}_{\boldsymbol{\psi}_k}, \mathbf{Q}_{\boldsymbol{\psi}_k}^{-1})$$

where  $\mathbf{Q}_{\boldsymbol{\psi}_k} = \sigma_\epsilon^{-2} (\mathbf{B}' \mathbf{B}) \sum_{i=1}^n \beta_{k,i}^2 + \lambda_{f_k} \boldsymbol{\Omega}$  and  $\boldsymbol{\ell}_{\boldsymbol{\psi}_k} = \sigma_\epsilon^{-2} \mathbf{B}' \sum_{i=1}^n \{\beta_{k,i} (\mathbf{y}_i - \mathbf{G}_\gamma \boldsymbol{\alpha}_i - \sum_{\ell \neq k} \mathbf{f}_\ell \beta_{\ell,i})\}$  (see Kowal and Bourgeois, 2020 for efficient techniques);

(b) Compute the constrained vector

$$\boldsymbol{\psi}_k = \boldsymbol{\psi}_k^0 - \mathbf{Q}_{\boldsymbol{\psi}_k}^{-1} \mathbf{C}_k' (\mathbf{C}_k \mathbf{Q}_{\boldsymbol{\psi}_k}^{-1} \mathbf{C}_k')^{-1} \mathbf{C}_k \boldsymbol{\psi}_k^0$$

where  $\mathbf{C}_k = (\mathbf{G}_\gamma, \mathbf{f}_1, \dots, \mathbf{f}_{k-1}, \mathbf{f}_{k+1}, \dots, \mathbf{f}_K)' \mathbf{B}$ ;

(c) Normalize:  $\beta_{k,i} \rightarrow \beta_{k,i} \|\mathbf{B} \boldsymbol{\psi}_k\|$ ,  $\boldsymbol{\psi}_k \rightarrow \boldsymbol{\psi}_k \|\mathbf{B} \boldsymbol{\psi}_k\|$ , and  $\mathbf{f}_k = \mathbf{B} \boldsymbol{\psi}_k$ ;

(d) Sample the smoothing parameter

$$[\lambda_{f_k}|] \sim \text{Gamma}((J+1)/2, \boldsymbol{\psi}_k' \boldsymbol{\Omega} \boldsymbol{\psi}_k / 2) \text{ truncated to } (10^{-8}, \infty)$$

where  $J$  is the number of columns of  $\mathbf{B}$ ;

4. **Ordered spike-and-slab parameters:** let  $y_{k,i}^F = \mathbf{f}_k' \mathbf{y}_i$  for  $i = 1, \dots, n$  and  $k = 1, \dots, K$ ;

(a) Sample  $[m_{\xi_{k,i}}|] \sim \text{Bernoulli}(1/(1 + \exp(-2\xi_{h,i})))$ ;

(b) Sample  $[\xi_{k,i}|] \sim N(Q_{\xi_{k,i}}^{-1} \ell_{\xi_{k,i}}, Q_{\xi_{k,i}}^{-1})$  where  $Q_{\xi_{k,i}} = \eta_k^2 / \sigma_\epsilon^2 + 1$  and  $\ell_{\xi_{k,i}} = \eta_k y_{k,i}^F / \sigma_\epsilon^2 + m_{\xi_{k,i}}$ ;

(c) Sample  $[\eta_k|] \sim N(Q_{\eta_k}^{-1} \ell_{\eta_k}, Q_{\eta_k}^{-1})$  where  $Q_{\eta_k} = \sum_{i=1}^n \xi_{k,i}^2 / \sigma_\epsilon^2 + (\theta_k \sigma_k^2)^{-1}$  and  $\ell_{\eta_k} = \sum_{i=1}^n \xi_{k,i} y_{k,i}^F / \sigma_\epsilon^2$ ;

(d) Rescale  $\eta_k \rightarrow (\sum_{i=1}^n |\xi_{k,i}| / n) \eta_k$  and  $\boldsymbol{\xi}_k \rightarrow (n / \sum_{i=1}^n |\xi_{k,i}|) \boldsymbol{\xi}_k$  and update  $\beta_{k,i} = \xi_{k,i} \eta_k$ ;

- (e) Sample  $[\sigma_k^{-2}|-] \sim \text{Gamma}\{a_1 + 1/2, a_2 + \eta_k^2/(2\theta_k)\}$ ;
- (f) Sample  $[\nu_k|-] \sim \text{Beta}(1 + \sum_{h=1}^K \mathbb{I}\{z_h = k\}, \kappa + \sum_{h=1}^K \mathbb{I}\{z_h > k\})$  for  $k = 1, \dots, K-1$  and update  $\omega_h = \nu_h \prod_{\ell=1}^{h-1} (1 - \nu_\ell)$  and  $\pi_k = \sum_{h=1}^k \omega_h$ ;
- (g) Sample  $[\kappa|-] \sim \text{Gamma}\{a_\kappa + K - 1, b_\kappa - \sum_{k=1}^{K-1} \log(1 - \nu_k)\}$ ;
- (h) Sample  $[z_k|-]$  from

$$\mathbb{P}(z_k = h|-) \propto \begin{cases} \omega_h t_{2a_1}(\eta_k; 0, \sqrt{v_0 a_2/a_1}) & h \leq k \\ \omega_h t_{2a_1}(\eta_k; 0, \sqrt{a_2/a_1}) & h > k \end{cases}$$

where  $t_d(x; m, s)$  is the density of the  $t$ -distribution evaluated at  $x$  with mean  $m$ , standard deviation  $s$ , and degrees of freedom  $d$ ;

- (i) **Update**  $\theta_k = 1$  if  $z_k > k$  and  $\theta_k = v_0$  if  $z_k \leq k$ .

5. **Parametric linear coefficients:** sample

$$[\boldsymbol{\alpha}_i|-] \stackrel{\text{indep}}{\sim} N(\mathbf{Q}_{\alpha_i}^{-1} \boldsymbol{\ell}_{\alpha_i}, \mathbf{Q}_{\alpha_i}^{-1}), \quad i = 1, \dots, n$$

where  $\mathbf{Q}_{\alpha_i} = \sigma_\epsilon^{-2} \mathbf{I}_L + \text{diag}(\{\sigma_{\alpha_\ell}^{-2}\}_{\ell=1}^L)$  and  $\boldsymbol{\ell}_{\alpha_i} = \sigma_\epsilon^{-2} \mathbf{G}'_\gamma \mathbf{y}_i$ ;

6. **Parametric variance:** using a parameter-expansion of the half-Cauchy distribution (Wand et al., 2011),

- (a) Sample  $[\sigma_{\alpha_\ell}^{-2}|- , \xi_{\sigma_{\alpha_\ell}}] \stackrel{\text{indep}}{\sim} \text{Gamma}((n+1)/2, \sum_{i=1}^n \alpha_{\ell,i}^2/2 + \xi_{\sigma_{\alpha_\ell}})$  for  $\ell = 1, \dots, L$ ;
- (b) Sample  $[\xi_{\sigma_{\alpha_\ell}}|\sigma_{\alpha_\ell}] \stackrel{\text{indep}}{\sim} \text{Gamma}(1, \sigma_{\alpha_\ell}^{-2} + 1)$  for  $\ell = 1, \dots, L$ ;

7. **Observation error variance:** sample

$$[\sigma_\epsilon^{-2}|-] \sim \text{Gamma}\left(nm/2, \sum_{i=1}^n \|\mathbf{y}_i - \mathbf{G}_\gamma \boldsymbol{\alpha}_i - \mathbf{F} \boldsymbol{\beta}_i\|^2/2\right).$$

## Hierarchical prior on the nonlinear parameter

For the pinch force data (Section 6.1), we include the hierarchical prior

$$\gamma_i \stackrel{iid}{\sim} N(\mu_\gamma, \sigma_\gamma^2), \quad \mu_\gamma \sim N(0, 10), \quad \sigma_\gamma \sim C^+(0, 1)$$

which requires minor modifications to the Gibbs sampling algorithm. The nonlinear parameter is still sampled using the slice sampler (Neal, 2003), but with the modified likelihood

$$p(\gamma_i | -) \propto p(\gamma_i | \mu_\gamma, \sigma_\gamma^2) \exp(-\frac{1}{2} \|\mathbf{y}_i - \mathbf{G}_\gamma \boldsymbol{\alpha}_i - \mathbf{F} \boldsymbol{\beta}_i\|^2 / \sigma_\epsilon^2)$$

specific to each  $i = 1, \dots, n$ , while the (conditional) prior is the aforementioned Gaussian distribution. The mean parameter is sampled from its full conditional distribution,

$$[\mu_\gamma | -] \sim N(Q_{\mu_\gamma}^{-1} \ell_{\mu_\gamma}, Q_{\mu_\gamma}^{-1}),$$

where  $Q_{\mu_\gamma} = n\sigma_\gamma^{-2} + 1/10$  and  $\ell_{\mu_\gamma} = \sigma_\gamma^{-2} \sum_{i=1}^n \gamma_i$ . The sampler for the standard deviation parameter uses a half-Cauchy parameter-expansion (Wand et al., 2011):

$$\begin{aligned} [\sigma_\gamma^{-2} | -, \xi_{\sigma_\gamma}] &\sim \text{Gamma}((n+1)/2, \sum_{i=1}^n (\gamma_i - \mu_\gamma)^2 / 2 + \xi_{\sigma_\gamma}) \\ [\xi_{\sigma_\gamma} | \sigma_\gamma] &\sim \text{Gamma}(1, \sigma_\gamma^{-2} + 1). \end{aligned}$$

## Dynamic models for the parametric factors

Since yield curve data (Section 6.2) are time-ordered for  $i = 1, \dots, n$ , we specified a dynamic model for the parametric factors

$$\alpha_{\ell,i} = \mu_\ell + \phi_\ell(\alpha_{\ell,i-1} - \mu_\ell) + \zeta_{\ell,i}, \quad \zeta_{\ell,i} \stackrel{\text{indep}}{\sim} N(0, \sigma_{\zeta_\ell}^2)$$

with the additional priors

$$\mu_\ell \stackrel{iid}{\sim} N(0, 10^6), \quad (\phi_\ell + 1)/2 \stackrel{iid}{\sim} \text{Beta}(5, 2), \quad \sigma_{\zeta_\ell} \stackrel{iid}{\sim} C^+(0, 1)$$

for  $\ell = 1, \dots, L$ . Conditional on  $\{\alpha_{\ell,i}\}$ , the sampling steps for these parameters are straightforward; see Kowal (2020) for details. Note that the prior on the (shifted and scaled) autoregression coefficients implies that the dynamic factors  $\{\alpha_{\ell,i}\}$  are stationary, and therefore so is the functional time series  $\{Y_i\}$ .

The dynamic factors can be sampled using state space simulation methods; we use Durbin and Koopman (2002) implemented in the KFAS package in R. Due to the orthogonality con-

straint  $\mathbf{G}'_\gamma \mathbf{F} = \mathbf{0}_{L \times K}$ , the observation equation simplifies to

$$\mathbf{y}_i = \mathbf{G}_\gamma \boldsymbol{\alpha}_i + \boldsymbol{\epsilon}_i, \quad \boldsymbol{\epsilon}_i \stackrel{\text{indep}}{\sim} N(\mathbf{0}, \sigma_{\epsilon_i}^2 \mathbf{I}_m)$$

for  $i = 1, \dots, n$ . The evolution equation is given by the independent AR(1) models for the dynamic factors  $\{\alpha_{\ell,i}\}_{i=1}^n$  for each  $\ell = 1, \dots, L$ . Using the state space construction, we can sample the factors  $\{\alpha_{\ell,i}\}$  jointly in  $O(nL^3)$  computational complexity.

The yield curve model also includes a stochastic volatility model on the observation error variance. The priors and sampling steps are identical to those in Kowal (2020).

## C Additional simulation results

### C.1 Inference for the parametric coefficients

Figure C.1 presents the mean credible interval widths and empirical coverage of the 95% posterior credible intervals for  $\{\alpha_{i,\ell}\}$  for  $K_{true} \in \{0, 3, 8\}$ . Although all models perform similarly in the parametric case ( $K_{true} = 0$ ), the SFFMs and the PFFM-gp offer much narrower interval estimates—while maintaining approximate nominal coverage—in the semiparametric case ( $K_{true} > 0$ ). The SFFMs further improve upon the PFFM-gp as  $K_{true}$  increases, and therefore provide more precise and correctly calibrated uncertainty quantification for the parametric coefficients. Note that point estimation accuracy for  $\{\alpha_{i,\ell}\}$  (not shown) is similar for all methods invariant of the true rank  $K_{true}$ .

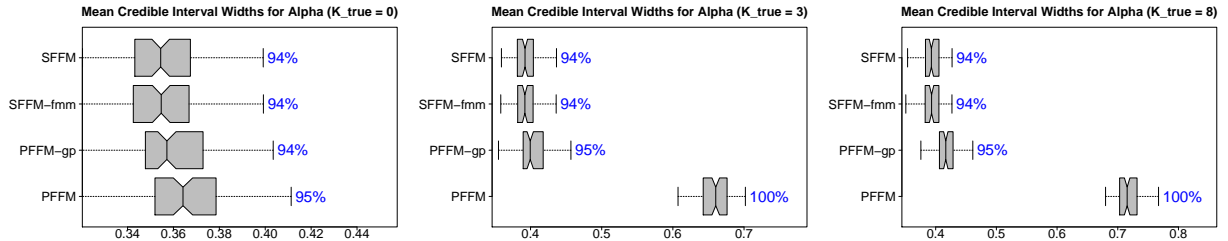


Figure C.1: Mean credible intervals widths and empirical coverage for  $\{\alpha_{i,\ell}\}$  for  $K_{true} = 0$  (left),  $K_{true} = 3$  (center), and  $K_{true} = 8$  (right). All models maintain approximately the nominal 95% coverage, but the prediction intervals for SFFM are substantially more narrow—and therefore more precise—when  $K_{true} > 0$ . Results for  $K_{true} = 1$  (omitted) are similar to those for  $K_{true} = 3$ .

## C.2 Linear template: $K_{true} = 8$

To assess performance in the presence of many nonparametric factors, we reproduce the simulation analysis from Section 5 in the case of  $K_{true} = 8$ . For the proposed SFFM and the finite mixture alternative (SFFM-fmm), we increase the bound on the number of factors from  $K = 10$  to  $K = 15$ . Figure C.2 consolidates the point prediction, interval prediction, and interval estimation results for the linear template; similar results are presented for the Nelson-Siegel template in Section C.3. The results are similar to those for  $K_{true} = 3$  in the main paper, and confirm the improvements offered by the SFFMs when  $K_{true} > 0$ .

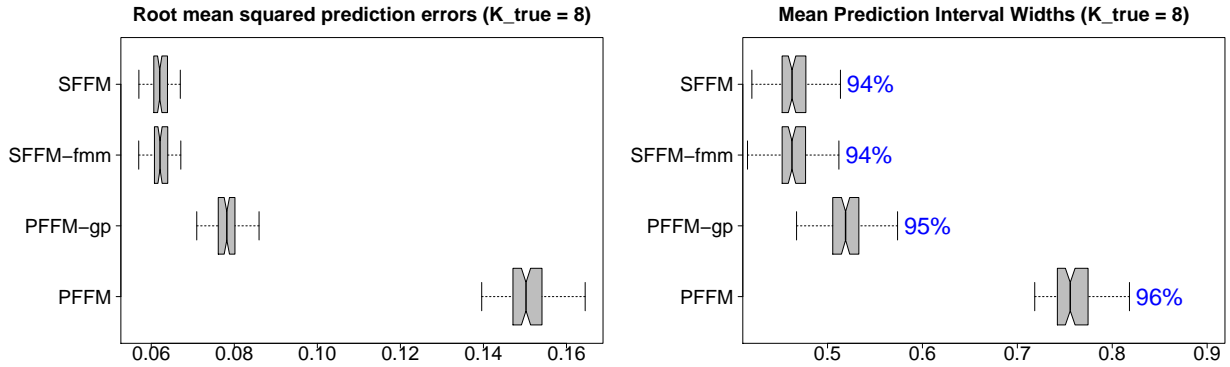


Figure C.2: Assessments of point prediction (left) and interval prediction (right) for  $K_{true} = 8$ . Results are similar to those for  $K_{true} = 3$ .

In Figure C.3, we revisit the comparisons between the SFFM and the SFFM-fmm for rank estimation and inference via  $\mathbb{P}(K^*|\mathbf{y})$ . For this more challenging scenario with  $K_{true} = 8$ , we find that it becomes more difficult to identify  $K_{true}$  and that the competing SFFM methodologies perform similarly.

## C.3 Nelson-Siegel template

We augment our simulation study to include the Nelson-Siegel template,

$$g_1(\tau; \gamma) = 1, \quad g_2(\tau; \gamma) = \{1 - \exp(-\tau\gamma)\}/(\tau\gamma), \quad g_3(\tau; \gamma) = g_2(\tau; \gamma) - \exp(-\tau\gamma)$$

with unknown  $\gamma > 0$ . The synthetic data-generating process proceeds as before, with following modifications: the true nonlinear parameter is set to  $\gamma^* = 0.0609$  (Diebold and Li, 2006; Bianchi et al., 2009) and the nonparametric basis matrix  $\mathbf{F}^*$  is orthogonalized to the parametric basis  $\mathbf{G}_{\gamma^*}^*$  using a QR-decomposition. As in the yield curve application, we use a

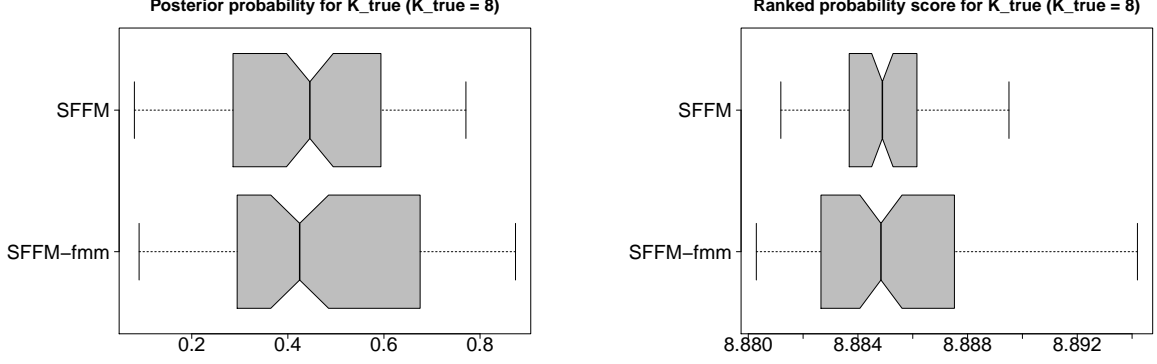


Figure C.3: Positively-oriented probability score  $\mathbb{P}(K^* = K_{true}|\mathbf{y})$  (left) and negatively-oriented ranked probability score for  $\mathbb{P}(K^*|\mathbf{y})$  (right) for the semiparametric functional factor models (SFFM) and the finite mixture model (SFFM-fmm) variant for  $K_{true} = 8$ . When the true nonparametric factor dimension is larger, it becomes more difficult to identify  $K_{true}$  and the differences between SFFM and SFFM-fmm are negligible.

Gamma prior for  $\gamma$  with prior mean 0.0609 and prior variance 0.5. The results are given in Figures C.4, C.5, and C.6 and confirm the results for the linear template in the main paper.

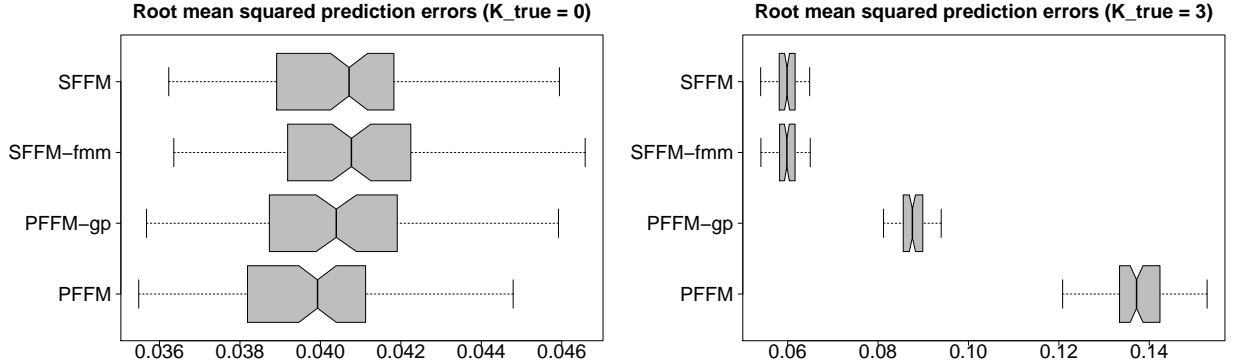


Figure C.4: Root mean squared prediction errors for  $Y^*$  for  $K_{true} = 0$  (left) and  $K_{true} = 3$  (right) under the Nelson-Siegel template. The SFFMs maintain point prediction accuracy in both settings, while the PFFM and PFFM-gp deteriorate substantially for  $K_{true} > 0$ . Results for  $K_{true} = 1$  are similar to those for  $K_{true} = 3$  and are omitted.

## C.4 Assessing inclusion probabilities for the nonparametric term

To further compare the SFFM and SFFM-fmm rank assessments, we study the probability of inclusion for *any* nonparametric terms,  $\mathbb{P}(K^* > 0|\mathbf{y})$ . When  $K_{true} > 0$ , we find that  $\mathbb{P}(K^* >$

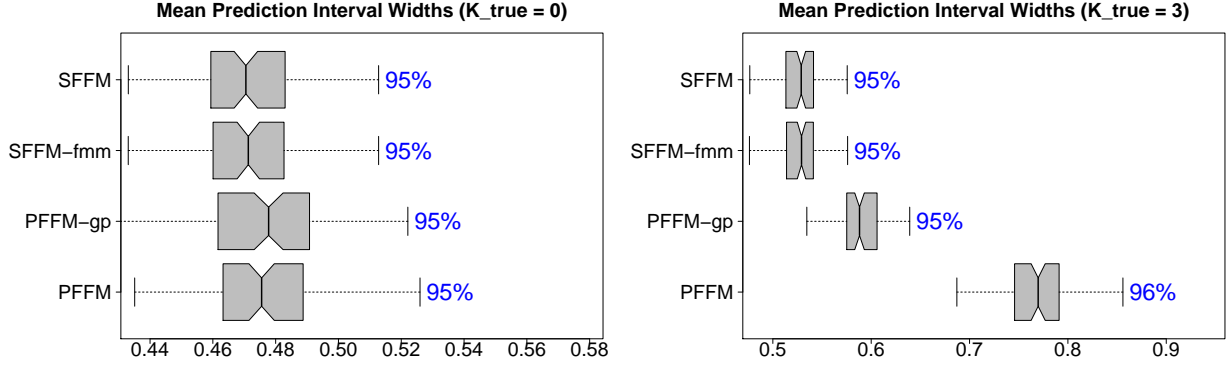


Figure C.5: Mean prediction interval widths and empirical coverage for  $K_{true} = 0$  (left) and  $K_{true} = 3$  (right) under the Nelson-Siegel template. All models maintain the nominal 95% coverage, but the prediction intervals for the SFFMs are substantially more narrow—and therefore more precise—when  $K_{true} > 0$ . Results for  $K_{true} = 1$  are similar to those for  $K_{true} = 3$  and are omitted.

$0|\mathbf{y}) = 1$  in all scenarios, so the SFFMs both offer excellent power for detecting the presence of a nonparametric addition. For the more challenging case of the true parametric model with  $K_{true} = 0$ , we report the summary statistics of  $\mathbb{P}(K^* > 0|\mathbf{y})$  across 100 simulations in Table C.1. The overestimation issues for the finite mixture alternative are apparent: compared to the SFFM, the SFFM-fmm assigns far greater inclusion probabilities for the nonparametric term when no such term is needed.

Template	Model	Min	1st quartile	Median	3rd quartile	Max
Linear	SFFM	0.070	0.117	0.142	0.183	0.370
	SFFM-fmm	0.123	0.229	0.280	0.354	0.642
Nelson-Siegel	SFFM	0.075	0.118	0.138	0.180	1.000
	SFFM-fmm	0.146	0.219	0.265	0.314	1.000

Table C.1: Summary statistics of  $\mathbb{P}(K^* > 0|\mathbf{y})$  across 100 simulations.



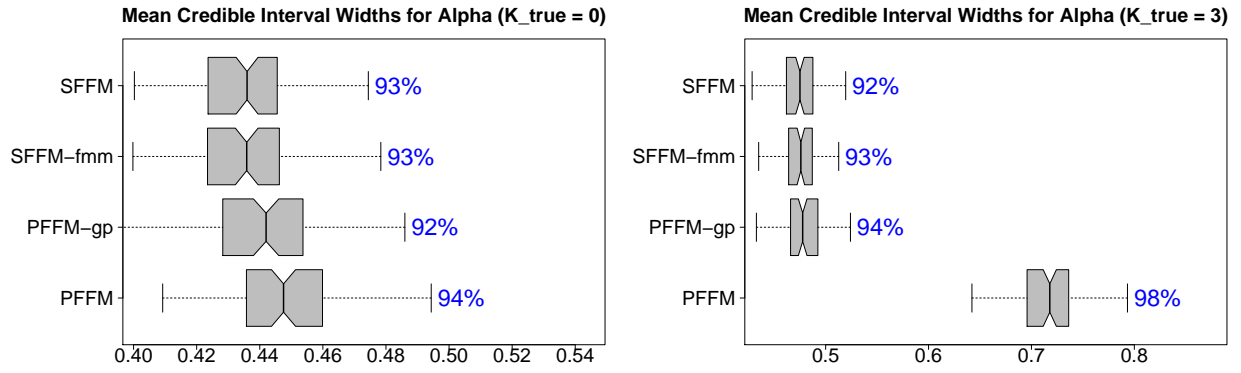


Figure C.6: Mean credible intervals widths and empirical coverage for  $\{\alpha_{i,\ell}\}$  for  $K_{true} = 0$  (left) and  $K_{true} = 3$  (right) under the Nelson-Siegel template. All models maintain approximately the nominal 95% coverage, but the prediction intervals for the SFFMs are substantially more narrow—and therefore more precise—when  $K_{true} > 0$ . Results for  $K_{true} = 1$  are similar to those for  $K_{true} = 3$  and are omitted.